

Sho1 and Msb2-Related Proteins Regulate Appressorium Development in the Smut Fungus *Ustilago maydis*

Daniel Lanver, Artemio Mendoza-Mendoza,¹ Andreas Brachmann,² and Regine Kahmann³

Max Planck Institute for Terrestrial Microbiology, D-35043 Marburg, Germany

The dimorphic fungus *Ustilago maydis* switches from budding to hyphal growth on the plant surface. In response to hydrophobicity and hydroxy fatty acids, *U. maydis* develops infection structures called appressoria. Here, we report that, unlike in *Saccharomyces cerevisiae* and other fungi where Sho1 (synthetic high osmolarity sensitive) and Msb2 (multicopy suppressor of a budding defect) regulate stress responses and pseudohyphal growth, Sho1 and Msb2-like proteins play a key role during appressorium differentiation in *U. maydis*. Sho1 was identified through a two-hybrid screen as an interaction partner of the mitogen-activated protein (MAP) kinase Kpp6. Epistasis analysis revealed that *sho1* and *msb2* act upstream of the MAP kinases *kpp2* and *kpp6*. Furthermore, Sho1 was shown to destabilize Kpp6 through direct interaction with the unique N-terminal domain in Kpp6, indicating a role of Sho1 in fine-tuning Kpp6 activity. Morphological differentiation in response to a hydrophobic surface was strongly attenuated in *sho1 msb2* mutants, while hydroxy fatty acid-induced differentiation was unaffected. These data suggest that Sho1 and the transmembrane mucin Msb2 are involved in plant surface sensing in *U. maydis*.

INTRODUCTION

A crucial step for phytopathogenic fungi to initiate infection of their hosts is the penetration of the plant cuticle. The most common strategy for entry into the plant tissue is the development of specialized infection structures known as appressoria (Tucker and Talbot, 2001). Appressorium formation is induced upon contact with the plant surface. The cues responsible for this differentiation range from chemical signals, such as ethylene, epicuticular waxes, and cutin monomers to the physical nature of the surface, such as hydrophobicity, hardness, and topography (Tucker and Talbot, 2001; Kumamoto, 2008). Processing of these signals depends on conserved signaling cascades. In *Magnaporthe oryzae* and *Botrytis cinerea*, cAMP signaling and mitogen-activated protein (MAP) kinase signaling are required for appressorium differentiation (Lee and Dean, 1993; Xu and Hamer, 1996; Choi and Dean, 1997; Zhao et al., 2005; Doehlemann et al., 2006). The involvement of MAP kinases in appressorium development has also been demonstrated in *Cochliobolus heterostrophus*, *Pyrenophora teres*, and *Colletotrichum* species (Lev et al., 1999; Kim et al., 2000; Takano et al., 2000; Ruiz-Roldan et al., 2001). While intracellular signaling

cascades have been linked to appressorium development in many phytopathogenic fungi, there is still poor knowledge about upstream receptors that regulate appressorial differentiation (Kumamoto, 2008). The only example so far is Pth11 (gene that plays a role in pathogenicity), a seven-transmembrane protein from *M. oryzae*. Pth11 has been suggested to be a surface sensor acting upstream of the cAMP pathway. However, *pth11* mutants are impaired in appressorium formation in response to both cutin monomers and hydrophobic surface cues (DeZwaan et al., 1999).

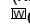
Ustilago maydis is the causative agent of maize (*Zea mays*) smut disease. A prerequisite for infection of its host plant maize is the fusion of two compatible cells, and this is achieved through a pheromone-receptor system (Bölker et al., 1992). The pheromone signal is transmitted through a MAP kinase cascade consisting of the MEKK (mitogen-activated protein kinase kinase kinase) Kpp4 (Andrews et al., 2000), the MEK (mitogen-activated kinase kinase) Fuz7 (Banuett and Herskowitz, 1994), and the MAP kinase Kpp2 (Mayorga and Gold, 1999; Müller et al., 1999, 2003). After cell fusion, a dikaryotic filament is established, which represents the infective form of *U. maydis* (Feldbrügge et al., 2004). In such filaments, the formation of septa leads to the accumulation of empty sections in the older parts of the filament. Only the growing tip cell is filled with cytoplasm and differentiates into an appressorium at appropriate sites on the plant surface (Snetselaar and Mims, 1992). In contrast with the dome-shaped, melanine-pigmented appressoria of *M. oryzae* and *Colletotrichum graminicola*, where high turgor pressure allows plant penetration predominantly by mechanical force (Howard et al., 1991; Bechinger et al., 1999), appressoria in *U. maydis* are only slightly swollen tips of the filaments, and penetration is thought to occur by secretion of lytic enzymes (Schirawski et al., 2005). Recent work demonstrated that a hydrophobic surface is essential and sufficient to induce not only septated filaments, but also appressorium formation in *U. maydis*, and addition of

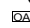
¹ Current address: Bio-Protection Research Centre, Lincoln University, Lincoln 7647, New Zealand.

² Current address: Ludwig-Maximilians-University München, Biozentrum Martinsried, Großhaderner Straße 2, D-82152 Martinsried, Germany.

³ Address correspondence to kahmann@mpi-marburg.mpg.de.

The author responsible for distribution of materials integral to the findings presented in this article in accordance with the policy described in the Instructions for Authors (www.plantcell.org) is: Regine Kahmann (kahmann@mpi-marburg.mpg.de).

 Online version contains Web-only data.

 Open Access articles can be viewed online without a subscription. www.plantcell.org/cgi/doi/10.1105/tpc.109.073734

hydroxy fatty acids strongly enhances appressorium formation efficiency (Mendoza-Mendoza et al., 2009b). The MAP kinase Kpp2 is involved in appressorium development (Müller et al., 2003), while another MAP kinase, Kpp6, which also acts downstream of Fuz7 (Di Stasio et al., 2009), is required for the appressorial penetration step (Brachmann et al., 2003; see Supplemental Figure 1A online). The morphological switch from budding to filamentous growth in response to the hydrophobic surface also depends on the MAP kinase Kpp2 (Mendoza-Mendoza et al., 2009b). However, the upstream receptors for the MAP kinase cascade that lead to appressorium development and penetration of the plant cuticle have not been identified so far.

The plasma membrane spanning protein Sho1 and the transmembrane mucin Msb2 are conserved proteins that serve as stress sensors in many fungal systems (Roman et al., 2005, 2009; Krantz et al., 2006; Norice et al., 2007; Ma et al., 2008; Boissard et al., 2008) and function upstream of MAP kinase cascades (Seet and Pawson, 2004; Cullen, 2007). In *Saccharomyces cerevisiae*, Sho1p and Msb2p were shown to interact and regulate signaling cascades involved in osmotic stress response and pseudohyphal growth (Chen and Thorner, 2007). In the high osmolarity glycerol (HOG) pathway, a SH3 (Src homology 3) domain-mediated interaction between Sho1p and the MEK Pbs2p leads to activation of the MAP kinase Hog1p (Brewster et al., 1993; Maeda et al., 1995). In the filamentous growth (FG) pathway, the MAP kinase Kss1p is phosphorylated by the MEK Ste7p (Liu et al., 1993; Roberts and Fink, 1994). In both pathways, upstream components are shared: The MEKK Ste11p activates Ste7p in the FG pathway as well as Pbs2p in the HOG pathway (Liu et al., 1993; Roberts and Fink, 1994; Posas and Saito, 1997). The tetraspan membrane protein Sho1p and the single transmembrane mucin Msb2p act at the head of the HOG and the FG pathway. While Sho1p interacts directly with Ste11p and Pbs2p, Msb2p is thought to function through the small GTPase Cdc42p and the PAK kinase Ste20p to activate Ste11p (Maeda et al., 1995; O'Rourke and Herskowitz, 1998; Cullen et al., 2004; Tatebayashi et al., 2007; see Supplemental Figure 1B online). *S. cerevisiae* possesses a second transmembrane mucin, Hkr1p, that acts in parallel with Msb2p in the HOG pathway but is dispensable for the FG pathway (Tatebayashi et al., 2007; Pitoniak et al., 2009).

In a previous study, a homolog of Sho1p was found to interact with the MAP kinase Kpp6 from *U. maydis* (Mendoza-Mendoza et al., 2009a). We also identified a transmembrane mucin with similarity to Msb2p from *S. cerevisiae* in the genome of *U. maydis* but no ortholog of Hkr1p. In this article, we demonstrate that Sho1 and Msb2 are crucial virulence factors that localize to the plasma membrane. Intriguingly, Sho1 and Msb2 proteins in *U. maydis* are not involved in stress responses but specifically regulate appressorium development in response to a hydrophobic surface by acting upstream of the MAP kinases Kpp2 and Kpp6.

RESULTS

The Plasma Membrane Protein Sho1 Interacts Specifically with the MAP Kinase Kpp6

By yeast two-hybrid screening, using the MAP kinase Kpp6 from *U. maydis* as bait, we identified the C-terminal domain of

Um03156 as putative interactor (Mendoza-Mendoza et al., 2009a). Um03156 encodes a 335-amino acid protein (<http://mips.gsf.de/genre/proj/ustilago/>) with similarity to the osmosensor Sho1p from *S. cerevisiae* (25% identity; Figure 1A). Sho1 and its orthologs in other fungi display an N-terminal secretion signal, four characteristic transmembrane domains, and a C-terminal

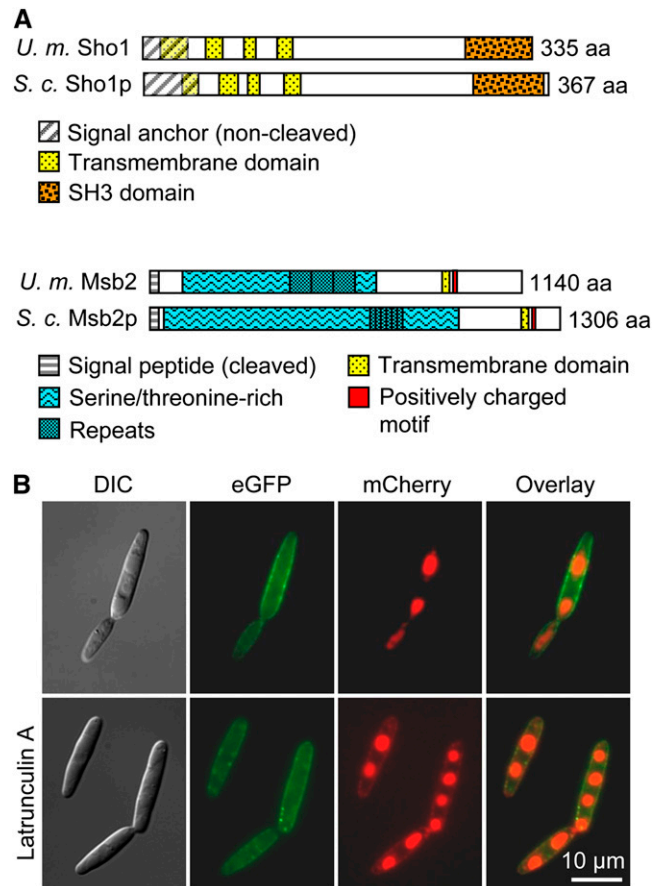


Figure 1. Domain Architecture and Localization of *U. maydis* Sho1 and Msb2.

(A) Top rows: Schematic representation of the domain structure of *U. maydis* Sho1 and *S. cerevisiae* Sho1p. Both proteins contain a non-cleaved secretion signal (SignalP), four transmembrane domains, of which the first is part of the secretion signal, and a C-terminal SH3 domain. Bottom rows: Schematic representation of the domain structure of *U. maydis* Msb2 and *S. cerevisiae* Msb2p. Msb2 of *U. maydis* and Msb2p of *S. cerevisiae* share common features of signaling mucins. They have a cleaved signal peptide (SignalP) and one transmembrane domain close to the N terminus. The large extracellular part is Ser/Thr rich and includes tandem repeats. The short cytoplasmic tail contains a positively charged motif (RKHRK in *U. maydis* Msb2; RRR in *S. cerevisiae* Msb2p). aa, amino acids.

(B) Localization of Sho1-GFP and Msb2-mCherry in *U. maydis*. SG200sho1GFP/msb2mCherry cells were grown to mid log phase in YEPSL and analyzed microscopically without addition (top row) or after addition of latrunculin (bottom row). The fluorescent signals corresponding to Sho1-GFP and Msb2-mCherry (middle columns) were merged (right column). Bright-field images are shown on the left.

SH3 domain. The Um03156 protein from *U. maydis* also displays such a domain structure and shows highest identity (61%) to Sho1p from yeast in the SH3 domain. Therefore, we designated *um03156* as *sho1*.

To determine the localization of Sho1 protein in *U. maydis*, a green fluorescent protein (*gfp*) tag was C-terminally fused to *sho1* in the native locus in the solopathogenic strain SG200. This fusion protein was biologically active (see below and Supplemental Figure 2A online). Sho1-GFP showed an asymmetric patchy distribution in the plasma membrane of the mother cells and only faint staining in the plasma membrane of daughter cells (Figure 1B). The subcellular localization of Sho1-GFP was also determined by cell fractionation. Sho1-GFP was exclusively found in the membrane fraction, confirming that Sho1 is a plasma membrane protein (see Supplemental Figure 3 online).

The interaction between Sho1 and Kpp6 was verified by *in vivo* coimmunoprecipitation. Since *kpp6* is not expressed in budding cells (Brachmann et al., 2003), a *myc-kpp6* fusion construct was placed under the control of the constitutively active *otef* promoter. This construct was integrated in multiple copies into the *ip* locus of SG200 Δ *kpp6* and SG200*sho1*GFP. Antibodies against the Myc-tag were used to precipitate Myc-Kpp6, and this weakly coprecipitated Sho1-GFP in SG200*sho1*GFP/*otef:kpp6-mc* (see Supplemental Figure 4A online).

To analyze whether the observed interaction between Sho1 and Kpp6 is specific, the yeast two-hybrid system was used. The coding region of four MAP kinases from *U. maydis* were cloned in the bait vector pGBKT7 and cotransformed with pGADT7-Sho1¹³¹⁻³³⁵ (see Supplemental Figure 4B online) into the *S. cerevisiae* strain AH109. The MAP kinases tested were the previously characterized kinases Kpp2 and Kpp6 (Mayorga and Gold, 1999; Müller et al., 1999; Brachmann et al., 2003), as well as Um02357, a MAP kinase related to Hog1p, and Um10107, a MAP kinase related to Slp2p. All strains showed similar expression levels of the respective MAP kinase proteins (see Supplemental Figure 4C online). The resulting strains were able to grow on selection plates; however, on high stringency plates, only the strain transformed with pGBKT7-Kpp6 and pGADT7-Sho1¹³¹⁻³³⁵ was able to grow (see Supplemental Figure 4D online), indicating that Sho1 and Kpp6 interact specifically.

***U. maydis* Encodes a Mucin-Like Protein**

In *S. cerevisiae*, Sho1p regulates filamentous growth and osmotic stress responses together with Msb2p (O'Rourke and Herskowitz, 2002; Cullen et al., 2004; Tatebayashi et al., 2007). The *U. maydis um00480* gene product showed significant similarity to yeast Msb2p (28% identity) as well as to proteins annotated as Msb2 orthologs in other fungi (Krantz et al., 2006) and was therefore designated Msb2. *msb2* encodes a putative protein of 1140 amino acids and contains all the classical characteristics described for transmembrane mucin proteins (Singh and Hollingsworth, 2006), such as an N-terminal signal sequence (amino acids 1 to 30), a Ser/Thr-rich domain (amino acids 108 to 692) that includes in the case of *U. maydis* Msb2 three identical repetitive domains of 69 amino acids each

(amino acids 430 to 636), and one transmembrane domain (amino acids 895 to 916) followed by a positively charged Lys/Arg-rich motif (RKHRK between amino acids 916 and 920; Figure 1A).

A biologically active C-terminal fusion of Msb2 (see below and Supplemental Figure 2A online) with the cherry fluorescent protein (mCherry) was generated in SG200*sho1*GFP to investigate putative colocalization of Msb2 and Sho1. The Msb2-mCherry fusion protein was concentrated in vacuoles but was absent from the plasma membrane (Figure 1B). We reasoned that this might result from a highly efficient actin-dependent endocytosis pathway and treated cells with latrunculin A, an inhibitor of actin polymerization. Latrunculin A has been demonstrated to efficiently inhibit endocytosis of the *U. maydis* pheromone receptor Pra1 (Fuchs et al., 2006). In latrunculin A-treated cells, the majority of Msb2-mCherry still localized to vacuoles, but under such conditions, a weak signal could additionally be detected in the plasma membrane and this signal colocalized with Sho1-GFP (Figure 1B).

Typically, cell surface-associated mucins are highly glycosylated and proteolytically cleaved, which separates the large extracellular part from the membrane-bound C terminus (Hollingsworth and Swanson, 2004). The predicted size of the Msb2-mCherry fusion protein is 145 kD. Immunoblotting revealed that the Msb2-mCherry protein is larger than 170 kD (see Supplemental Figure 3 online). Furthermore, a 65-kD fragment that could represent a specific C-terminal cleavage product of Msb2-mCherry was detected. The full-length protein as well as the C-terminal fragment were mainly found in the membrane fraction and only to a minor extent in the cytoplasm (see Supplemental Figure 3 online). These results indicate that *U. maydis* Msb2 is a membrane-associated mucin.

***sho1* and *msb2* Are Not Required for Mating and Do Not Affect Stress Responses**

To investigate the function of *sho1* and *msb2* in *U. maydis*, deletion mutants and double deletion mutants were generated in the compatible haploid strains FB1 and FB2 as well as in the solopathogenic strain SG200 using a one-step gene replacement procedure (Kämper, 2004). Haploid deletion derivatives were tested for mating by cospotting cultures on potato dextrose (PD) charcoal plates. After 48 h, all strain combinations had developed vigorous dikaryotic hyphae that gave the colonies a fuzzy appearance. However, the mating response of crosses with Δ *sho1* Δ *msb2* strains was slightly less efficient than in combinations with *sho1* and *msb2* single mutants or wild-type strains (see Supplemental Figure 5A online). When SG200 and the SG200 mutant derivatives were spotted on PD charcoal plates, SG200 Δ *sho1* Δ *msb2* showed slightly reduced filamentation after 24 h (Figure 2A). These results likely reflect that *sho1* and *msb2* are not required for a successful cell fusion reaction while the development of dikaryotic hyphae is slightly attenuated in the absence of both genes.

In *S. cerevisiae*, *Candida albicans*, and *Aspergillus fumigatus*, deletion of putative orthologs of *sho1* resulted in strains with increased sensitivity to oxidative and osmotic stress as well to cell wall interfering compounds like congo red and calcofluor

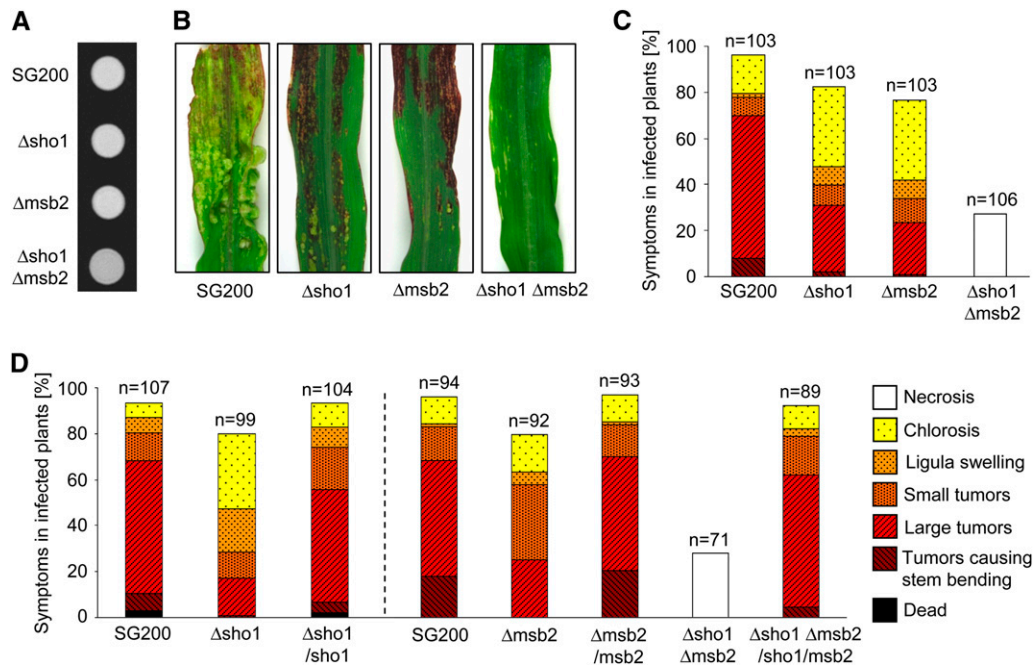


Figure 2. Pathogenicity of *sho1* and *msb2* Mutant Strains in the SG200 Background.

(A) The solopathogenic strain SG200 and its derivatives indicated below were spotted on PD charcoal plates and incubated for 24 h at 28°C. The white fuzzy colonies reflect the formation of *b*-dependent filaments.

(B) Representative leaves 12 d after infection with the indicated strains.

(C) Disease symptoms caused by SG200, *sho1*, and *msb2* single mutants and *sho1 msb2* double mutants in the SG200 background. The indicated strains were injected into maize seedlings and symptoms were scored 12 d after infection. Based on the severity of symptoms observed on each plant, symptoms were grouped into color-coded categories according to Kämper et al. (2006). Colors and patterns for disease scores are indicated to the right of **(D)**. Three independent experiments were performed and the average values are expressed as a percentage of the total number of infected plants (n), which is given above each column. Tested strains are listed below each column.

(D) Complementation of SG200-derived *sho1* and *msb2* single and double mutants. Plants were infected with the indicated strains and evaluated as described in **(C)**.

(Maeda et al., 1995; Roman et al., 2005; Ma et al., 2008). To investigate whether *sho1* and *msb2* in *U. maydis* contribute to growth under stress conditions, serial dilutions of SG200, the *sho1* and *msb2* mutant derivatives, as well as the *sho1 msb2* double mutant were plated on agar containing the respective stressors. Growth on these plates was indistinguishable between mutant strains and SG200 on media containing congo red (70 μ g/mL), calcofluor (50 μ M), H_2O_2 (1.5 mM), NaCl (1 M), sorbitol (2 M), and water agar containing 1% glucose (see Supplemental Figure 6A online). Under nitrogen limiting conditions, *S. cerevisiae* switches from bipolar budding to pseudohyphal growth, and this process depends on Sho1p and Msb2p (Gimeno et al., 1992; Cullen et al., 2004). *U. maydis* also grows filamentously on low ammonium medium (Smith et al., 2003). To test if Sho1 and Msb2 have a function during this process, the colony morphology of SG200, the *sho1* and *msb2* single mutant derivatives as well as the *sho1 msb2* double mutant were analyzed on nitrogen limiting medium (SLAHD). All strains showed a filamentous colony morphology after 36 h (see Supplemental Figure 6B online). This indicates that contrary to the situation in *S. cerevisiae* and other fungi, *sho1* and *msb2* in *U. maydis* do not participate in stress sensing.

sho1 and *msb2* Are Required for Pathogenic Development in *U. maydis*

To analyze the role of *sho1* and *msb2* during pathogenic development, 7-d-old maize plants were infected with SG200, SG200 Δ *sho1*, SG200 Δ *msb2*, and SG200 Δ *sho1* Δ *msb2*. Disease symptoms were scored after 12 d according to severity (Kämper et al., 2006), and averages from three independent experiments are shown (Figure 2). Compared with SG200, a decreased tumor rate was observed in infections with SG200 Δ *sho1* and SG200 Δ *msb2*, and in both cases, the percentage of plants with severest disease symptoms was most strongly reduced (Figures 2B and 2C). Interestingly, SG200 Δ *sho1* Δ *msb2* was unable to cause tumors and instead necrotic lesions were observed (Figures 2B and 2C). To verify the reduced virulence independently, maize plants were infected with compatible mixtures of wild-type and *sho1* or *msb2* deletion strains, respectively (see Supplemental Figure 5B online). While the overall symptom severity was higher than in SG200 and its derivatives, single *sho1* or single *msb2* mutants were again attenuated in virulence. In crosses between FB1 Δ *sho1* Δ *msb2* and FB2 Δ *sho1* Δ *msb2*, neither tumor formation nor chlorosis was observed and instead

necrotic lesions developed (see Supplemental Figure 5B online), which corroborates the findings for SG200 Δ sho1 Δ msb2.

To complement the *sho1* and *msb2* single mutants, either *sho1* or *msb2* was reintroduced in single copy in the *ip* locus of the respective SG200-derived deletion strains. In the resulting strain SG200 Δ msb2/*msb2*, virulence could be completely restored, while in SG200 Δ sho1/*sho1*, complementation levels were slightly lower (Figure 2D). To explain this, we speculate that the *sho1* locus contains regulatory upstream or downstream elements that are missing in the complementation construct. To demonstrate that the loss of virulence in SG200 Δ sho1 Δ msb2 resulted only from disruption of *sho1* and *msb2*, a *sho1 msb2* double construct was integrated in single copy in the *ip* locus of the *sho1 msb2* double mutant. In this strain, virulence was almost completely restored (Figure 2D). The slight attenuation compared with SG200 is likely due to incomplete complementation by the *sho1* gene (see above).

To investigate what is underlying the induction of necrotic lesions after infection with SG200 Δ sho1 Δ msb2, infected leaves were harvested after 3 d and stained with propidium iodide and calcofluor. Calcofluor allows detection of the fungal material on the leaf surface, while the non-membrane-permeable propidium iodide stains plant cell walls and DNA, if the membrane is ruptured (i.e., in dead plant cells). In infections with SG200, the propidium iodide stain was almost exclusively found in the plant cell walls, while after infection with SG200 Δ sho1 Δ msb2, plant cell walls in the infected area were more strongly stained, plant cell nuclei were brightly stained, and these cells showed internal blue staining presumed to reflect autofluorescence (see Supplemental Figure 7 online). This indicates that the Δ sho1 Δ msb2 mutant elicits plant defense responses associated with plant cell death.

To elucidate at which developmental stage the mutants are affected, the infected plant areas were stained with carbohydrate binding wheat germ agglutinin–alexa fluor conjugate (WGA-AF488) and analyzed by confocal microscopy 6 d after inoculation. Massive intracellular fungal proliferation was observed in leaves infected with SG200, while leaves infected with SG200 Δ sho1 or SG200 Δ msb2 showed reduced fungal material (Figure 3A). By contrast, after infection with SG200 Δ sho1 Δ msb2, only very few intracellular hyphae could be detected (Figure 3A). To quantify fungal biomass, leaves of infected plants were detached 3 d after infection, fungal cells on the surface were removed by latex treatment and total DNA was extracted. Relative fungal biomass was determined by quantitative real-time PCR using the fungal *mfa1* gene and the plant GAPDH gene as internal standards (Figure 3B). *sho1* and *msb2* single mutants were about twofold and threefold reduced in fungal biomass, respectively, compared with SG200, while the double mutant showed a reduction of about fivefold (Figure 3B). Because of the severely reduced amount of intracellular fungal material, we consider it likely that the *sho1 msb2* double mutant is affected in a step prior to or during penetration.

Appressorium Development Is Regulated by *sho1* and *msb2*

To address whether filamentation on the leaf surface and appressorium formation were affected by *sho1* and/or *msb2* dele-

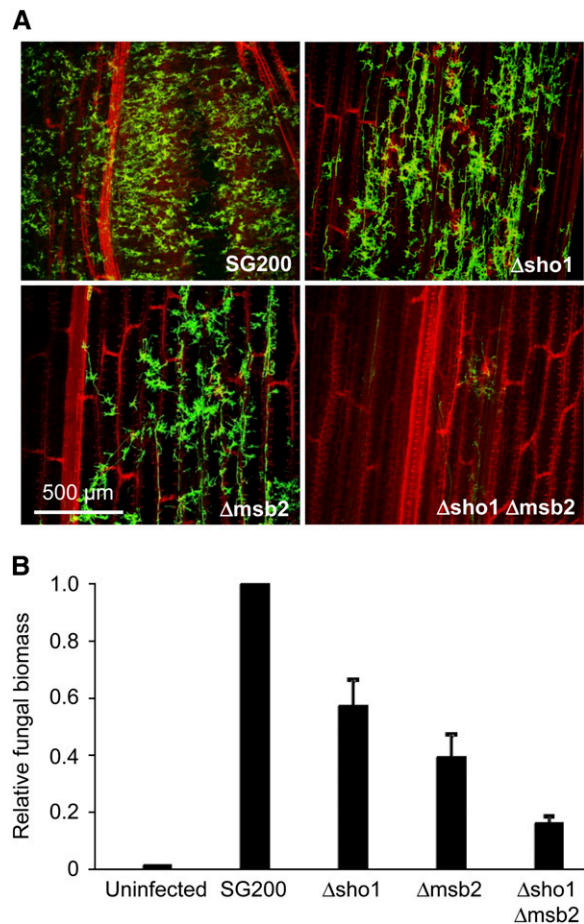


Figure 3. Host Colonization Is Impaired in *sho1* and *msb2* Mutants.

(A) Confocal projections of representative leaves 6 d after infection with the indicated strains. Plant tissue is shown at the layer of vascular bundles. Fungal material was stained by WGA-AF488 (green). Plant material was stained by propidium iodide (red).

(B) Quantification of fungal biomass by quantitative PCR. *U. maydis*-specific and plant-specific primers were used to determine the relative fungal biomass in plants 3 d after infection with the indicated strains. Columns give ratios of fungal DNA to plant DNA, and the ratio in SG200-infected plants was set to 1.0. Means of three independent experiments with 30 leaves per strain are shown, and error bars indicate standard deviations.

tion, we introduced the AM1 marker, which is a promoter fused to a triple *gfp* that is specifically upregulated in those hyphal cells that differentiate appressoria (Mendoza-Mendoza et al., 2009b). Calcofluor staining revealed that SG200AM1, *sho1*, and *msb2* single as well as double mutant strains showed comparable filamentation on the leaf surface (Figure 4A). However, when the percentage of hyphae that had developed appressoria was determined 18 h after inoculation, both SG200AM1 Δ sho1 and SG200AM1 Δ msb2 were significantly reduced in appressorium formation compared with SG200AM1, while SG200AM1 Δ sho1 Δ msb2 did not develop any appressoria (Figures 4A and 4B).

We recently established *in vitro* conditions for filamentation and appressorium development: filaments resembling conjugation tubes can be induced in SG200 by 16-hydroxyhexadecanoic acid, while hydrophobicity induces filaments with empty sections. On the hydrophobic surface, a few appressoria are induced and this level is strongly enhanced when 16-hydroxyhexadecanoic acid is added (Mendoza-Mendoza et al., 2009b). The *sho1* and *msb2* single mutant as well as the double mutant responded to 16-hydroxyhexadecanoic acid like the parental strain SG200 (Figure 5A; see Supplemental Figure 8 online). On the hydrophobic surface, SG200 Δ *sho1* Δ *msb2* was affected in filamentation, while the *sho1* and *msb2* single mutants

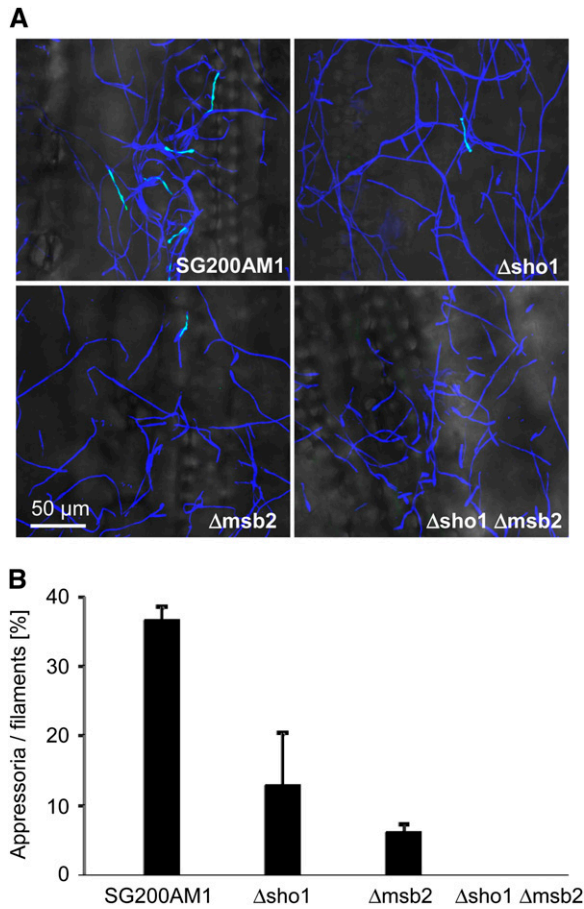


Figure 4. Sho1 and Msb2 Affect Appressorium Formation on the Plant Surface.

(A) Maize seedlings were infected with SG200AM1 and its derivatives as indicated. Eighteen hours after infection, the surface of the third oldest leaf was analyzed by confocal microscopy. Fungal hyphae were stained by calcofluor (blue), and expression of the AM1 marker (green) indicates appressorium formation. The overlays of maximum projections of both channels with the corresponding bright-field images are depicted.

(B) Quantification of appressoria on the plant surface. Using the same strains as in **(A)**, the average percentage of filaments that had formed appressoria to the total number of filaments was determined. For each strain (indicated below each column), >900 filaments were analyzed in three independent experiments. Error bars indicate standard deviations.

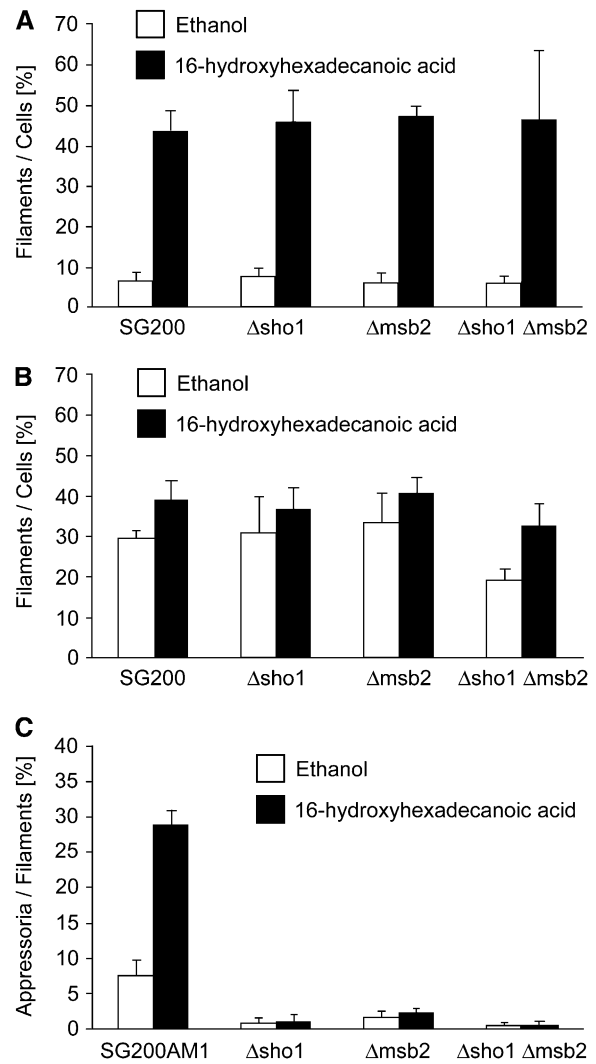


Figure 5. *sho1* and *msb2* Mutants Respond to Hydroxy Fatty Acid but Are Impaired in Their Response to Hydrophobic Surfaces.

(A) Filamentation in liquid: The indicated strains (below each column) were tested for their response to 16-hydroxyhexadecanoic acid. Cells were incubated in liquid culture (2% YEPLS) supplemented with either 100 μ M 16-hydroxyhexadecanoic acid dissolved in ethanol (black columns) or with ethanol (white columns) for 18 h at 28°C. The average percentage of cells that grew filamentously was determined by microscopy analysis.

(B) Filamentation on a hydrophobic surface: Cell suspensions of the indicated strains in 2% YEPLS were sprayed on Parafilm M with 100 μ M 16-hydroxyhexadecanoic acid dissolved in ethanol (black columns) or with ethanol (white columns) and incubated for 18 h at 28°C. After staining of fungal cells with calcofluor, the average percentage of cells that grew filamentously was determined microscopically.

(C) Appressorium formation on a hydrophobic surface: SG200AM1 and its derivatives indicated below the columns were sprayed on a hydrophobic surface as described in **(B)**, incubated for 18 h at 28°C, and stained with calcofluor. After microscopy analysis, the average percentage of cells that expressed the AM1 marker was determined relative to the cells that had formed filaments.

In three independent experiments, >900 cells **(A)** and **(B)** or filaments **(C)** per strain were analyzed, and error bars indicate standard deviations.

reacted like the progenitor strain (Figure 5B; see Supplemental Figure 9 online). The addition of 16-hydroxyhexadecanoic acid enhanced filamentation in all mutant strains as described previously for SG200 (Mendoza-Mendoza et al., 2009b). However, with respect to appressorium development on the hydrophobic surface, the *sho1* and *msb2* single as well as the double mutant were severely reduced, and the addition of 16-hydroxyhexadecanoic acid had only a slight enhancing effect in the single mutants and no effect in the double mutant (Figure 5C; see Supplemental Figure 9 online). This shows that *sho1* and *msb2* specifically affect development of appressoria. Therefore, we determined the localization of Sho1-GFP during appressorium formation. Sho1-GFP showed a patchy distribution in filaments but accumulated strongly in appressoria (Figures 6A and 6B). Attempts to visualize Msb2-mCherry in filaments failed due to the background fluorescence of the inducing surface. To enhance expression of *msb2-mCherry*, we placed the gene under the control of the constitutively active *otef* promoter (Spellig et al., 1996) and integrated this construct into the *ip* locus in strains SG200 Δ *msb2* and SG200*sho1*GFP. The construct was able to complement SG200 Δ *msb2* (see Supplemental Figure 2B online). In filaments, Msb2-mCherry accumulated in vacuoles that were distributed throughout the filament. In appressoria, Msb2-mCherry strongly accumulated in vacuoles (Figures 6A and 6C), corroborating a function of Msb2 during this stage of development. Colocalization with Sho1-GFP was not apparent (Figure 6D).

Sho1 and Msb2 Act Upstream of the MAP Kinases Kpp2 and Kpp6

In *U. maydis*, the MAP kinase Kpp2 is implicated in appressorium development induced by the hydrophobic stimulus (Müller et al., 2003; Mendoza-Mendoza et al., 2009b), while the related MAP kinase Kpp6 is specifically needed for appressorium function (Brachmann et al., 2003). The dual specificity phosphatase Rok1 is a negative regulator of the MAP kinases Kpp2 and Kpp6, and deletion of *rok1* leads to hypervirulence (Di Stasio et al., 2009). To test whether activated Kpp2 and Kpp6 restore tumor development in SG200 Δ *sho1* Δ *msb2*, we deleted *rok1* in this strain. While plants infected with SG200 Δ *sho1* Δ *msb2* showed no tumor development 12 d after infection, SG200 Δ *sho1* Δ *msb2* Δ *rok1*-infected plants developed tumors and symptom severity was comparable to SG200 infections (Figure 7). To substantiate that Sho1 and Msb2 activate the MAP kinase module containing Kpp2 and Kpp6 and to rule out the possibility that *rok1* suppresses the virulence phenotype of the Δ *sho1* Δ *msb2* mutant by a mechanism that is independent of Kpp2 and Kpp6, we integrated the constitutively active version of the MEK *fuz7* (*fuz7DD*; Müller et al., 2003) under the control of the arabinose-inducible *crg1* promoter in the genome of SG200 Δ *sho1* Δ *msb2* as well as in the genome of SG200. Expression of *fuz7DD* was induced by adding arabinose to the inoculum prior to infection of maize plants. As a control, arabinose was replaced by glucose, which represses the activity of the *crg1* promoter (Bottin et al., 1996). When SG200*fuz7DD* was used to infect maize plants, symptom development was comparable irrespective of whether glucose or arabinose was added to the inoculum (Figure 8A). SG200 Δ *sho1*

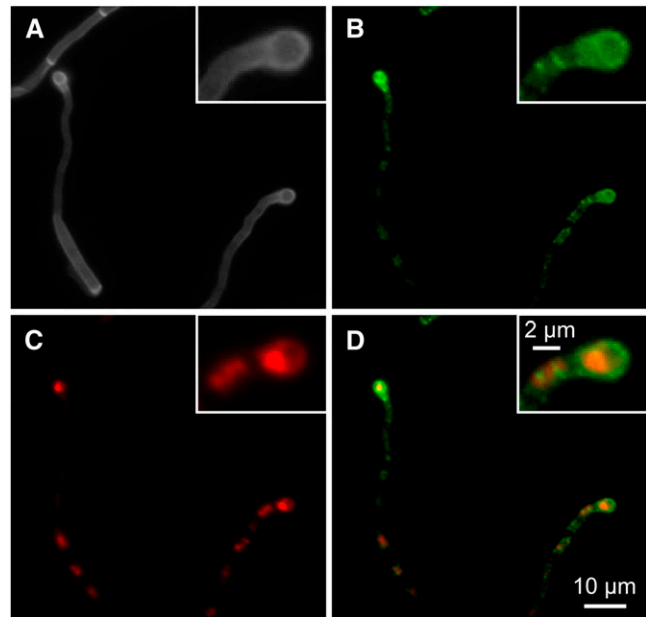


Figure 6. Localization of Sho1-GFP and Msb2-mCherry in Appressoria.

(A) to (D) SG200*sho1*GFP/*otef*:*msb2*mCherryHA was sprayed with 100 μ M 16-hydroxyhexadecanoic acid on paraffin wax and incubated as described in Figure 5B. A section displaying two appressoria is analyzed. The appressorium on the right-hand side is magnified in the inset.

(A) Calcofluor staining.

(B) Visualization of Sho1-GFP (green).

(C) Visualization of Msb2-mCherry (red).

(D) Overlay of (B) and (C).

Δ *msb2* *fuz7DD* induced necrosis when glucose was added (Figures 8A and 8B). However, when arabinose was added as an inducer for *fuz7DD*, we observed chlorotic areas and anthocyanin production, which is indicative of successful penetration (Figures 8A and 8C). Microscopy analysis of leaves 6 d after infection confirmed that penetration had occurred and the amount of fungal material inside the leaf was much more abundant when *fuz7DD* was induced compared with the repressed situation (Figures 8B and 8C). These data indicate that Sho1 and Msb2 act upstream of the MAP kinases Kpp2 and Kpp6.

Functional Analysis of Msb2

If Msb2 functions as a cell surface receptor, the transmembrane domain should be important for function. To test this hypothesis, the transmembrane domain within the *otef*:*msb2-mCherryHA* construct was deleted and the construct integrated in the *ip* locus of SG200 Δ *msb2*. Plant infections revealed that *msb2* Δ *TM-mCherry-ha* could not complement the virulence defect of the *msb2* deletion strain (see Supplemental Figure 10A online). Furthermore, only the full-length protein could be detected in immunoblot analysis, whereas the C-terminal Msb2-mCherryHA fragment was absent (see Supplemental Figure 10B online). These results indicate that the transmembrane domain of Msb2 is essential for processing and function of Msb2.

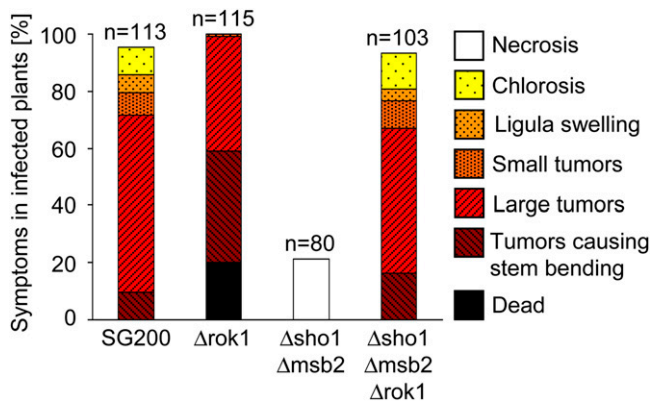


Figure 7. The Deletion of *rok1* Suppresses the Virulence Phenotype of SG200Δ*sho1* Δ*msb2*.

Maize plants were infected with SG200 and the indicated derivatives. Disease rating was done as described in the legend to Figure 2. Tested strains are listed below each column, the numbers of infected plants (*n*) are given above each column, and the color and pattern code for disease rating is depicted on the right.

U. maydis Msb2 and *S. cerevisiae* Msb2p have similar domain structures but display only 28% amino acid identity (Figure 1A). To address whether *U. maydis* *msb2* is able to complement the *S. cerevisiae* *msb2* mutant, we made use of the yeast strain PC538 that is defective in the mating pathway and has a *FUS1:HIS3* reporter whose expression is driven only by the FG pathway (Cullen et al., 2004). The PC538 derivative PC948 carries the *msb2* deletion and is hence unable to grow on medium without His (Cullen et al., 2004). *U. maydis* *msb2* and *S. cerevisiae* *MSB2* were inserted under the control of the constitutively active *ADH1* promoter into the free replicating plasmid pVTU260 and transformed into PC948. Expression of *U. maydis* Msb2 was verified by immunoblot analysis (see Supplemental Figure 11A online). *S. cerevisiae* strain PC948, expressing *U. maydis* *msb2*, was unable to grow on medium lacking His, while *S. cerevisiae* *MSB2* could complement the growth phenotype of the *msb2* deletion strain (see Supplemental Figure 11B online). This demonstrates that, although characteristic features are shared between the Msb2 proteins in *U. maydis* and *S. cerevisiae*, they do not represent functional homologs.

The SH3 Domain of Sho1 Interacts with a Negative Regulatory Domain of Kpp6

To establish the biological significance of the observed interaction between Sho1 and Kpp6, we delineated the region responsible for the interaction between Kpp6 and Sho1. Different segments of Sho1 and Kpp6 were tested by two-hybrid interaction for their ability to interact with each other. In all cases, the amounts of fusion proteins expressed were comparable (see Supplemental Figure 12A online). We found that Kpp6 interacted specifically with the SH3 domain of Sho1 (amino acids 279 to 335), while the linker domain (amino acids 131 to 278) that is situated between the SH3 domain and the fourth transmembrane

domain showed no interaction with Kpp6. With respect to Kpp6, we mapped the interaction domain to amino acids 1 to 170, which constitutes the unique N-terminal domain of Kpp6 (see Supplemental Figures 12B and 12C online). Based on the knowledge that SH3 domains interact with Pro-rich domains (PRDs; Li, 2005), we searched for such a motif in the N terminus of Kpp6. This led to the identification of the motif KPLPPSP (corresponding to amino acids 127 to 133), which conforms to type I PRDs (R/KxxPxxP; Li, 2005). To test the functional significance of this motif in Kpp6, we generated a mutant in which two

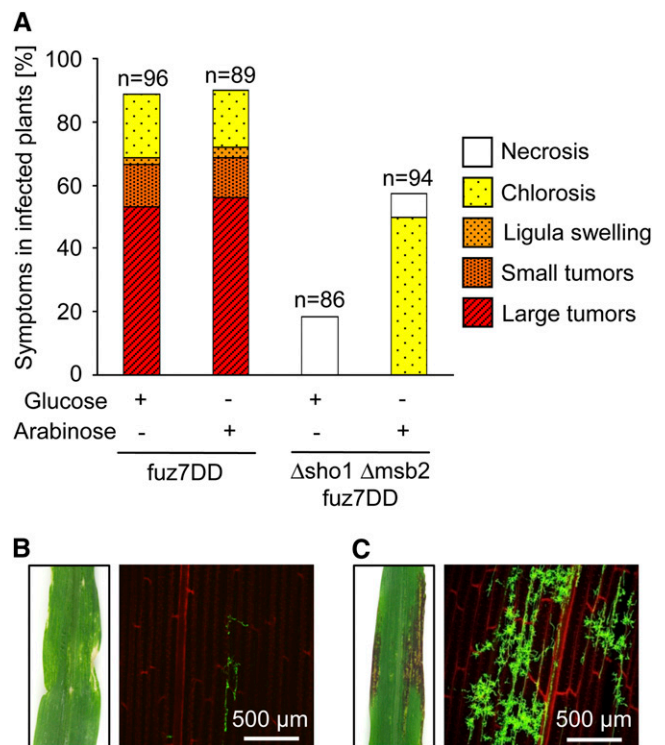


Figure 8. Expression of a Constitutively Active Allele of *fuz7* Partially Bypasses the Need for Sho1 and Msb2.

(A) The indicated SG200 derivatives were inoculated into maize seedlings. Prior to infection, either arabinose (to induce *fuz7DD* expression) or glucose (to repress *fuz7DD* expression) was added to the inoculums to a final concentration of 1%. Twelve days after infection, symptoms were scored as described in the legend to Figure 2. Inoculated strains and glucose/arabinose supplements are listed below each column, numbers of infected plants (*n*) are given above each column, and the color and pattern code for disease rating is depicted on the right.

(B) Macroscopy and microscopy symptoms after infection with SG200Δ*sho1* Δ*msb2* *fuz7DD* in the presence of glucose. A representative infected leaf is shown on the left 12 d after infection. Confocal microscopy performed as described in the legend to Figure 3A reveals poor colonization of plant tissue 6 d after infection (right panel).

(C) Macroscopy and microscopy symptoms after infection with SG200Δ*sho1* Δ*msb2* *fuz7DD* in the presence of arabinose. A representative infected leaf 12 d after infection is shown on the left. Confocal microscopy performed as described in legend to Figure 3A reveals strongly enhanced colonization of plant tissue 6 d after infection (right panel).

Pro residues are substituted by Ala (KPLAASP). Two-hybrid interactions demonstrated that Kpp6^{P130A P131A} is no longer able to interact with the SH3 domain of Sho1 despite similar expression levels of the respective fusion proteins (see Supplemental Figure 12 online).

To test whether the observed interaction of Sho1 and Kpp6 is relevant for pathogenic development of *U. maydis*, a *sho1* allele lacking the SH3 domain (*sho1*^{Δ280-335}) was generated in the endogenous locus in SG200. Pathogenicity assays revealed that this mutant was attenuated in virulence to a level slightly above that observed in the *sho1* deletion mutant (see Supplemental Figure 13 online). With respect to the functional relevance of the interaction domain in Kpp6, we generated alleles in which either the N-terminal domain was deleted or the PR motif was mutated. To avoid problems associated with the complex regulation of *kpp6* (Brachmann, 2001), these alleles were expressed from the constitutive *otef* promoter and carried an N-terminal *myc* tag. A derivative of SG200Δ*kpp6* expressing N-terminally *myc*-tagged wild-type *kpp6* from the *otef* promoter (*otef:kpp6*) served as control. In this control strain, partial complementation of the *kpp6* deletion phenotype was observed (Figure 9A). In SG200Δ*kpp6*

derivatives expressing *kpp6*^{P130A P131A}, virulence was elevated compared with SG200Δ*kpp6*/*otef:kpp6*, and the expression of *kpp6*^{Δ1-169} in SG200Δ*kpp6* led to a further increase in virulence (Figure 9A). However, when the same *kpp6* alleles were introduced in SG200Δ*sho1* Δ*kpp6*, which is unable to cause disease (Figure 9A), symptom development was restored to the same extent with both the wild-type allele and the *kpp6*^{P130A P131A} allele (Figure 9A). On the other hand, introduction of the *kpp6*^{Δ1-169} allele into SG200Δ*sho1* Δ*kpp6* led again to increased virulence compared with that of *kpp6* or *kpp6*^{P130A P131A}. The virulence-enhancing effect of the *kpp6*^{Δ1-169} allele was significantly higher in the Δ*sho1* Δ*kpp6* background than in the Δ*kpp6* background (Figure 9A). This illustrates that the N terminus of Kpp6 as well as the PRD alone have a negative role during virulence. In the absence of *sho1*, the negative effect of the PRD alone was no longer visible. To elucidate the basis for these findings, we determined the Kpp6 protein levels of the various strains (Figure 9B). This revealed that Kpp6^{P130A P131A} levels were significantly higher than Kpp6 levels in the Δ*kpp6* strain background. By contrast, in the Δ*sho1* Δ*kpp6* strain background, Kpp6 and Kpp6^{P130A P131A} protein levels were comparable and as high as

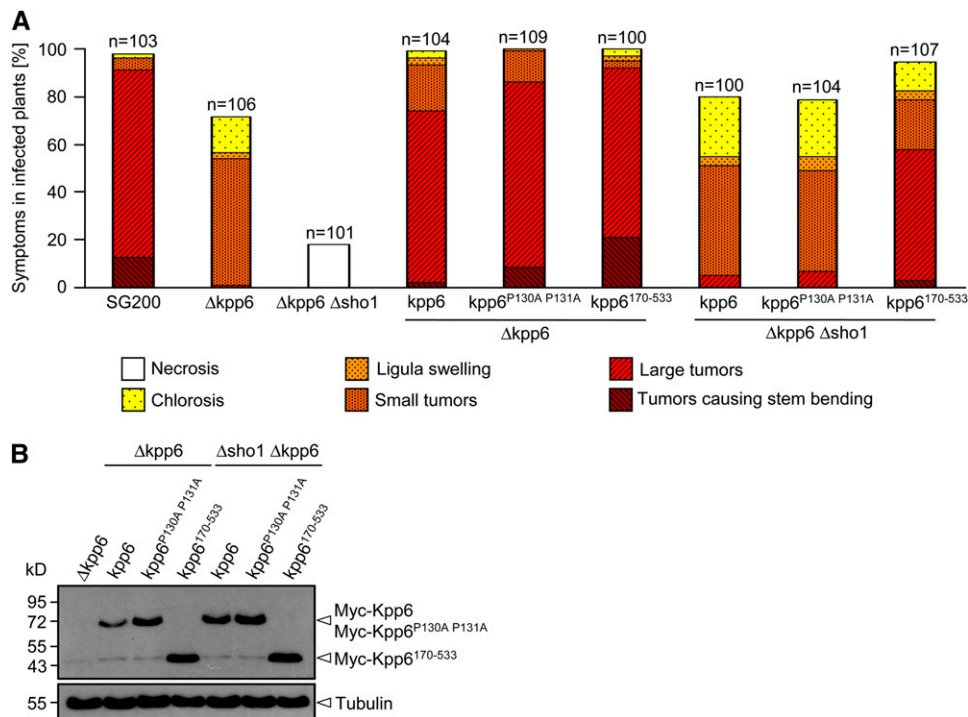


Figure 9. The Interaction of Sho1 and Kpp6 Influences Pathogenicity.

(A) Wild-type *kpp6*, *kpp6*^{P130A P131A}, and N-terminally truncated *kpp6*^{Δ1-169} were constitutively expressed as N-terminal Myc-fusion proteins in either SG200Δ*kpp6* or SG200Δ*sho1* Δ*kpp6*. The SG200 derivatives listed below each column were inoculated into maize seedlings, and symptoms were scored 12 d after infection as described in the legend to Figure 2.

(B) The indicated SG200Δ*kpp6*- and SG200Δ*sho1* Δ*kpp6*-derived strains were grown in liquid YEPSL to an OD₆₀₀ of 1.0, and proteins were extracted and subjected to SDS-PAGE. After blotting, anti-Myc was used to detect Myc-Kpp6 as well as its mutated and truncated alleles (top panel). The Myc antibody detects with low signal intensity one unspecific cross-hybridizing protein at the size of Myc-Kpp6^{Δ1-169} that was disregarded. Tubulin served as loading control and was detected with antitubulin (bottom panel). The fusion proteins and tubulin are indicated by arrowheads on the right. The molecular mass marker is depicted on the left.

the Kpp6^{P130A P131A} levels in the $\Delta kpp6$ strain background (Figure 9B). Compared with the Kpp6^{P130A P131A} level, the amount of the truncated version Kpp6 ^{Δ 1-169} was further elevated and was indistinguishable in the $\Delta kpp6$ and $\Delta sho1 \Delta kpp6$ strain background (Figure 9B). This suggests that Sho1 negatively influences the stability of Kpp6 through direct interaction with the N terminus of Kpp6.

DISCUSSION

In this article, we showed that Sho1 and Msb2 in *U. maydis* are essential virulence factors. *sho1* and *msb2* mutants are specifically reduced in pathogenic development and are not significantly affected in mating and stress responses. The virulence defects could be traced back to a failure in developing appressoria.

Using bioinformatic tools, Msb2 of *U. maydis* was recently classified as an ortholog of *S. cerevisiae* Msb2p (Krantz et al., 2006). Complementation studies have now shown that these proteins are not functional homologs, which is not unexpected, in view of the light that they regulate distinct processes in both organisms (see below). Nevertheless, with respect to domain structure, Msb2p from *S. cerevisiae* and Msb2 from *U. maydis* are clearly related (Figure 1A). For Msb2p in *S. cerevisiae*, it has been demonstrated that the extracellular domain is highly *N*- as well as *O*-glycosylated (Cullen et al., 2004; Yang et al., 2009), and using the program NetNGlyc 1.0 (<http://cbs.dtu.dk/services/NetNGlyc/>), seven *N*-glycosylation sites in *U. maydis* Msb2 (eight in *S. cerevisiae* Msb2p) were predicted. Furthermore, the combination of all six recommended constraints of the program OGPET 1.0 (<http://ogpet.utep.edu/OGPET/>) predicts an average of 12 *O*-glycosylation sites for Msb2 in *U. maydis* (nine for *S. cerevisiae* Msb2p). We consider it likely that Msb2 in *U. maydis* is a glycosylated transmembrane mucin. This assertion is supported by the finding that its apparent molecular mass of >170 kD is significantly higher than its expected mass of 147 kD as well as the finding that the transmembrane domain is crucial for Msb2 function.

While Sho1- and Msb2-related proteins serve as stress sensors in all fungal systems analyzed to date (Maeda et al., 1995; O'Rourke and Herskowitz, 2002; Roman et al., 2005, 2009; Norice et al., 2007; Boisnard et al., 2008; Ma et al., 2008), *sho1* and *msb2* are not needed for general stress responses in *U. maydis*. Responses to osmotic stress, oxidative stress, or cell wall stress were not altered in *sho1* and *msb2* single or double mutants, suggesting that the function of Sho1 and Msb2 in *U. maydis* is uncoupled from the HOG pathway and serves in pathogenicity only.

In *U. maydis*, pathogenic development is initiated by *b*-dependent filaments, which are septated and accumulate empty sections. On the plant surface, *sho1* and *msb2* mutants were able to form these filaments as efficiently as the progenitor strain. However, single deletion mutants in *sho1* or *msb2* showed reduced colonization of the plant tissue, and the *sho1 msb2* double deletion mutant had an almost complete colonization defect. The quantification of appressoria on the plant surface revealed that single deletion strains of *sho1* or *msb2* form fewer appressoria than SG200, and the *sho1 msb2* double deletion

strain was not able to form appressoria. Thus, Sho1 and Msb2 have cooperative and essential functions during appressorium development. Interestingly, mutants lacking an ortholog to *MSB2* in *Fusarium oxysporum* showed delayed invasive growth and were strongly attenuated in virulence (E. Perez-Nadales and A. Di Pietro, personal communication), suggesting that mucins may have a general function during the early infection stages of phytopathogenic fungi.

We observed strong plant defense responses when the *sho1 msb2* double mutant grows on the leaf surface. This most likely reflects pathogen-associated molecular pattern-induced defense responses that are suppressed after wild-type hyphae penetrate the epidermal layer (Doehlemann et al., 2008a). Due to the penetration defect, the *sho1 msb2* double mutant would be unable to suppress this reaction. The failure of the *sho1 msb2* mutant to develop appressoria is at variance with results that rely on fungal biomass determinations. In these experiments, only a fivefold reduction in colonization was observed relative to the progenitor strain SG200. In addition, confocal microscopy allowed us to detect rare colonization events by the *sho1 msb2* mutant. We consider intracellular fungal biomass determination during early infection stages to be error prone as it relies on complete removal of fungal hyphae from the leaf surface by latex treatment. To explain the rare colonization successes of the *sho1 msb2* mutant, we speculate that this reflects the ability of *U. maydis* to enter plant tissue as a saprophyte without the formation of appressoria. This could actually be facilitated by dead plant cells as they are found underneath SG200 $\Delta sho1 \Delta msb2$ cells growing on the leaf surface.

In yeast, Msb2p has been shown to interact with Sho1p (Cullen et al., 2004). Attempts to visualize an interaction between Sho1 and Msb2 in *U. maydis* relying on epitope-tagged proteins and coimmunoprecipitations were unsuccessful. This could suggest that interactions are only transient and may be restricted to appressoria (i.e., a stage not yet accessible to biochemical analysis). Msb2p of yeast has also been demonstrated to interact with Cdc42p, and this complex is hypothesized to provide sensory capacity in the FG pathway that is transmitted via the PAK kinase Ste20p (Cullen et al., 2004). In *U. maydis*, Cdc42 is part of a signaling module consisting of the Rho-GEF Don1 and the Ste20-like kinase Don3 (Weinzierl et al., 2002). While *don3* mutants are not affected in pathogenic development (Weinzierl et al., 2002), *cdc42* mutants are nonpathogenic (Mahlert et al., 2006). A second PAK in *U. maydis*, Cla4, a member of the Cla4 subfamily of Ste20-like kinases, is involved in the regulation of cell polarity during budding and filamentation and *cla4* mutants are nonpathogenic (Leveleki et al., 2004). It will be interesting to determine whether pathogenicity defects of *cdc42* and *cla4* mutants occur at the stage of appressorium formation as this could provide a direct link to Sho1 and Msb2.

Recently, the dual specificity phosphatase Rok1 has been characterized as a negative regulator of Kpp2 and Kpp6. Deletion of *rok1* results in hypervirulence, which can be partially explained by increased appressorium formation (Di Stasio et al., 2009). When the *rok1* gene was deleted in the $\Delta sho1 \Delta msb2$ background, the resulting strain became fully pathogenic, indicating that Sho1 and Msb2 feed into the Kpp2/Kpp6 MAP kinase cascade, and a lack of this input can be compensated for by the

deletion of *rok1*. This is corroborated by demonstrating that expression of the constitutively active allele of the MEK Fuz7 that activates the MAP kinases Kpp2 and Kpp6 (Müller et al., 2003; Di Stasio et al., 2009) allowed to bypass the colonization defect of the *sho1 msb2* deletion strain. Since tumor formation was not observed when *fuzDD* was induced by arabinose prior to infection with SG200 Δ *sho1* Δ *msb2* *fuz7DD*, this most likely indicates that *fuz7DD* expression ceases after penetration (due to insufficient amounts of arabinose in the plant tissue) and that Sho1 and Msb2 have additional, Fuz7-dependent functions during the biotrophic phase. Since *U. maydis* appears to require the formation of appressoria for cell-to-cell passages (Doehlemann et al., 2009), it is conceivable that the reinitiation of this program is affected in the *sho1 msb2* double mutant. Overall, these results place Sho1 and Msb2 upstream of Kpp2 and Kpp6, where they function as sensors to activate MAP kinase signaling.

An intriguing feature of this signaling pathway is that Sho1 protein was identified as a two-hybrid interactor of Kpp6 (Mendoza-Mendoza et al., 2009a). We demonstrated here that this interaction occurs via the SH3 domain of Sho1 and the PR-motif in Kpp6. This motif is located in the N-terminal extension of Kpp6, which is absent from Kpp2 (Brachmann et al., 2003). *kpp6* is strongly upregulated in *b*-dependent filaments and is specifically needed for appressoria to penetrate (Brachmann et al., 2003). The finding that a *kpp6* allele that lacks the N-terminal domain is significantly stronger in complementing the pathogenicity defect of *kpp6* mutants than wild-type *kpp6* suggests that the N terminus of Kpp6 has an inhibitory function. A Kpp6 variant that no longer interacts with Sho1 due to mutations in the PR domain also causes enhanced virulence and this effect requires Sho1. The demonstration that Kpp6 protein levels are elevated when the PRD is mutated or *sho1* is deleted makes it likely that the interaction with Sho1 destabilizes Kpp6. We speculate that the interaction with Sho1 could impose a negative feedback loop that might fine-tune Kpp6 levels during the differentiation of appressoria. In *S. cerevisiae*, it has been demonstrated that a negative feedback loop exists between Sho1p and Hog1p that is based on phosphorylation of Sho1p by Hog1p (Hao et al., 2007). The cytoplasmic domain of *U. maydis* Sho1 contains three putative MAP kinase phosphorylation sites. However, simultaneous mutation of all three sites did not affect virulence of the respective strain (D. Lanver and R. Kahmann, unpublished data), making a phosphorylation-based feedback loop unlikely. Despite the negative function of the PRD in the N terminus of Kpp6, this domain must additionally confer regulatory information. This is based on the observation that the deletion of the entire N terminus causes stronger virulence than mutating only the PRD in Kpp6. Furthermore, in this case, the enhanced virulence does not depend on Sho1.

The deletion of the SH3 domain in *sho1* reduces virulence to a similar extent as disruption of the entire *sho1* gene. Thus, the negative effect of the SH3 domain of Sho1 on Kpp6 levels cannot be the only function of this domain. In yeast, the MEK Pbs2p is recruited to the plasma membrane via interaction of the Sho1p SH3 domain with the Pro-rich motif KPLPPLP in the N terminus of Pbs2p (Maeda et al., 1995; Raitt et al., 2000; Reiser et al., 2000). In *U. maydis*, the MEK Fuz7 acts downstream of Sho1. Since

Fuz7 lacks such a Pro-rich motif and we currently have no evidence that Sho1 and Fuz7 interact, further experimentation will be necessary to link the SH3 domain in Sho1 to components of the MAP kinase module.

In *S. cerevisiae*, activation of Msb2 is regulated by starvation-dependent induction of its cognate aspartyl protease Yps1p (Vadaie et al., 2008). Yps1p processes Msb2p into a secreted extracellular form and a cell-associated form. This cleavage releases the inhibitory mucin domain and generates the active form of Msb2 (Vadaie et al., 2008). Our finding of two forms of Msb2 in *U. maydis*, a high molecular mass form and a form representing the C terminus also suggests a processing event. However, we currently have no indication that the extracellular domain in Msb2 assumes a negative regulatory function. In *S. cerevisiae*, Msb2-GFP localizes primarily to vacuoles, and this localization depends on efficient processing of Msb2p (Vadaie et al., 2008). Given that *U. maydis* Msb2-mCherry also accumulates in vacuoles in the appressorium, we speculate that Msb2 could be activated when appressoria are formed.

Recently, Msb2p in *S. cerevisiae* has been identified as a target for the mannosyltransferase Pmt4p and deletion of *pmt4* leads to underglycosylated Msb2p, as well as to enhanced activity of the FG pathway (Yang et al., 2009). Interestingly, the deletion of *pmt4* in *U. maydis* causes a specific defect in appressorium development, while vegetative growth and filament formation are not affected (Fernandez-Alvarez et al., 2009). Since Msb2 is an upstream component of the MAP kinase cascade regulating appressorium development, Msb2 is likely to be a mannosylated target of Pmt4 in *U. maydis*.

In *U. maydis*, appressoria can be efficiently induced on a hydrophobic surface when hydroxy fatty acids are added (Mendoza-Mendoza et al., 2009b). In contrast with the situation on the leaf surface, in vitro appressorium formation was not only abolished in *sho1 msb2* double mutants, but already in *sho1* and *msb2* single mutants. This could indicate that on the plant surface additional signals are provided that allow *sho1* and *msb2* single mutants to form appressoria. Under the in vitro conditions, *sho1* and *msb2* mutants were able to develop filaments in response to hydroxy fatty acids alone, indicating that this pathway is unaffected. Formation of septated filaments by the *sho1 msb2* double mutant occurred inefficiently on the hydrophobic surface but was increased when hydroxy fatty acids were added. We take this to indicate that the hydrophobic surface is only poorly sensed. Moreover, with respect to the in vitro differentiation of appressoria, the *sho1* and *msb2* mutants are defective. We speculate that the reduced response to hydrophobicity of *sho1* and *msb2* mutants in vitro results from inefficient perception of the hydrophobic stimulus. As this is the crucial signal for appressorial differentiation (Mendoza-Mendoza et al., 2009b), the reduced perception could translate into the complete failure to form these infection structures. So far, it is not entirely clear what is sensed by Sho1p/Msb2p in *S. cerevisiae* (Cullen, 2007). The physical properties of the heavily glycosylated extracellular domains of mucins change dramatically in response to changes in extracellular milieu, and in higher eukaryotes, mucins have been shown to bind to and detect the presence of eukaryotic cells, proteins, and microorganisms (De Nadal et al., 2007). We consider these properties to be extendable to abiotic surface

recognition, although formal proof for this needs further experimentation.

METHODS

Strain Construction and Growth Conditions

The *Escherichia coli* strains DH5 α (Bethesda Research Laboratories) and Top10 (Invitrogen) were used for cloning purposes. The *Saccharomyces cerevisiae* strain AH109 (Clontech) was used for two-hybrid interaction studies. The *S. cerevisiae* strains PC538 and PC948 (Cullen et al., 2004) were used for *msb2* complementation studies. All *S. cerevisiae* strains are listed in Supplemental Table 1 online.

Ustilago maydis strains were grown in liquid YEPSL (0.4% yeast extract, 0.4% peptone, and 2% sucrose) or on solid potato dextrose (PD) plates. For mating assays and filament induction, PD plates containing 1% activated charcoal were used (Holliday, 1974).

Haploid *U. maydis* strains FB1 and FB2, and solopathogenic strains SG200, SG200AM1, SG200 Δ kpp6, and SG200 Δ rok1 have been described previously (Banuett and Herskowitz, 1989; Brachmann et al., 2003; Kämper et al., 2006; Di Stasio et al., 2009; Mendoza-Mendoza et al., 2009b).

For gene disruptions, the PCR strategy described by Kämper (2004) and the *SfiI* insertion cassette system (Brachmann et al., 2004) were used. All gene replacement constructs were sequenced after cloning. After transformation, DNA gel blot analysis was performed to confirm gene replacements or insertions. All *U. maydis* strains are listed in Supplemental Table 2 online.

For generation of *sho1* (*um03156*) deletion mutants, two 1.0-kb fragments containing the 5' flanking region and the 3' flanking region of the *sho1* gene were amplified by PCR using FB1 genomic DNA as template with the primer combinations oAM150/oAM151 (5'-GAGTCTTGACTGTTCGCGATAC-3'/5'-CACGGCCTGAGTGGCCAGCATGCCTGGTTCAGCCAGCTG-3') for the left border and oAM152/oAM153 (5'-GTGGGCCATCTAGGCCGAGATCGAGCTGGTCTATAC-3'/5'-CGACGACTTGTGGAGTTGGCC-3') for the right border. The PCR fragments were digested with *SfiI* and ligated to the hygromycin resistance cassette isolated as a 2.7-kb *SfiI* fragment from plasmid pMF1-h (Brachmann et al., 2004). The ligation product was cloned into pCRII-TOPO (Invitrogen) to obtain p Δ sho1-Hyg. The plasmid was digested with *Eco0109I* and *HindIII* prior to transformation in SG200. The 2.7-kb hygromycin cassette of p Δ sho1-Hyg was replaced by the 1.4-kb nourseothricin resistance cassette from pMF1-n (Brachmann et al., 2004), resulting in p Δ sho1-Nat. This plasmid was digested with *PstI* and *BamHI* before transformation and was used for *sho1* disruption in FB1, FB2, and SG200 Δ kpp6.

For deletion of only the SH3 domain of *sho1*, the primer combination oDL02/oDL03 (5'-TAGAAGCTTCTGTCCACAGCTTGGCTG-3'/5'-TATGGCGCGCCCTAGTAGCCGTAGTCGGGCAG-3') was used to amplify the 5' region of *sho1*. Primer oDL03 introduces a stop codon at amino acid position 280, just before the SH3 domain starts. The PCR product was digested with *AsclI*. The 3' flanking region of *sho1* was amplified using the primers oDL04 (5'-GATGAGCTCCGAGATCGAGCTGGTCTATACC-3') and oDL05 (5'-ATCAAGCTTCGACGACTTGTGGAGTTGG-3'), following digestion with *SacI*. A three-fragment ligation including a 3.0-kb *AsclI/SacI* fragment containing the *nos* terminator and the hygromycin resistance cassette, the PCR fragments corresponding to the 3' flanking region of *sho1* and to the C-terminally truncated *sho1* gene was performed. The ligation product was cloned into pCRII-TOPO to obtain psho1 Δ 280-335. The plasmid was digested with *HindIII* and transformed in SG200, resulting in strain SG200sho1 Δ 280-335.

To generate *msb2* (*um00480*) deletion mutants, two 1.0-kb fragments comprising the 5' flank and the 3' flank of the *msb2* gene were generated

by PCR with the primer pairs oOM1/oOM2 (5'-TACACCTCATCATT-CACGCTAACGC-3'/5'-CACGGCCTGAGTGGCCAAAGAGACAAGTGGGAGGCTGACG-3') and oOM3/oOM4 (5'-GTGGGCCATCTAGGCCTGT-TTGCTTTGGTTGTAACGGAACG-3'/5'-TGTCTGGCTGCACCACTCTATTACG-3'). The PCR products were digested with *SfiI* and ligated with the 1.9-kb *SfiI* hygromycin resistance cassette from pBS-hhn (Kämper, 2004). The resulting product was cloned into pCRII-TOPO to generate p Δ msb2-Hyg, which was digested with *HindIII* and *XbaI* and transformed in SG200, FB1, and FB2. To generate *sho1* and *msb2* double deletions strains, the 1.9-kb hygromycin resistance cassette of p Δ msb2-Hyg was replaced by the 1.9-kb carboxin resistance cassette of pBS-Cbx (Kämper, 2004) to yield p Δ msb2-Cbx. Prior to transformation in FB1 Δ sho1 and FB2 Δ sho1, the plasmid was digested with *HindIII* and *XbaI*. For generation of SG200 Δ sho1 Δ msb2, the PCR-amplified *msb2* borders were ligated with the 1.4-kb nourseothricin resistance cassette from pMF1-n and the ligation product cloned into pJet1 (Fermentas). Prior to transformation in SG200 Δ sho1, the plasmid was digested with *BspEI* and *PvuII*.

To complement SG200 Δ sho1 with *sho1*, a 1.9-kb fragment corresponding to the promoter and the open reading frame (ORF) of *sho1* was amplified using primers oAM154 (5'-CGCTCGGTACCCGGTG-ATTTGTGATTAACACGTC-3') and oDL01 (5'-CTAGGCGCGCCCTATAGGAGCTGCATGTAGTTGCTG-3'), following digestion with *AsclI*. p123 (Aichinger et al., 2003) was linearized with *NotI* and refilled with Klenow according to the recommendations of the manufacturer (New England Biolabs). Then, the linearized plasmid was cut with *Acc65I* and the 4.7-kb *Acc65I*/blunt fragment was ligated with the 1.9-kb *Acc65I*/blunt *sho1* fragment. The resulting plasmid, p123P_{sho1:sho1}, contains the ORF of *sho1* under the control of its own promoter and the *nos* terminator. p123P_{sho1:sho1} was linearized with *SspI* and transformed into SG200 Δ sho1. Single-copy integrations in the *ip* locus were identified as described previously (Loubradou et al., 2001).

For construction of the *msb2* complementation plasmid, p123 was digested with *NdeI* and *NotI*, and the 4.5-kb fragment was ligated with the 6.9-kb *NdeI/NotI* fragment corresponding to the promoter and the ORF of *msb2*, which was amplified using the primers oAM288 (5'-GCCCGCATATGGCTGATGAAGAAAGAGCACT-3') and oAM290 (5'-GCCTGCGGCCGATTTAAAGGAGAACCAGAGTTG-3'). p123P_{msb2:msb2} contains the ORF of *msb2* under the control of its own promoter and the *nos* terminator. For complementation, plasmid p123P_{msb2:msb2} was linearized with *SspI* and integrated in single copy in the *ip* locus of SG200 Δ msb2. For complementation of the *sho1* *msb2* double mutant, p123P_{sho1:sho1} was digested with *PvuII* and *HpaI*, and the 2.3-kb fragment corresponding to the promoter, the *sho1* gene, and the *nos* terminator were ligated into *HpaI*-linearized p123P_{msb2:msb2}. The resulting plasmid p123P_{sho1:sho1}-P_{msb2:msb2} was integrated in single copy into the *ip* locus of SG200 Δ sho1 Δ msb2.

To generate SG200sho1GFP, a 1.0-kb left border corresponding to the coding region of *sho1* was amplified using the primers oDL08 (5'-GGTGGCCGCGTTGGCCCGCTCGATCGCCACCGGTAGGAGCTGCATGTAGTTGCTGGG-3') and oDL02. The right border was amplified using the primers oDL05 and oDL09 (5'-ATAGGCCTGAGTGGCCGAGATCGAGCTGGTCTATAC-3'). Both fragments were digested with *SfiI* and ligated with the 3.7-kb *SfiI* fragment from pBS-eGFP, which contains the *egfp* gene, the *nos* terminator, and the hygromycin resistance cassette (Brachmann, et al., 2004). The ligation product was cloned in pCRII-TOPO to yield psho1-eGFP. In this plasmid, the *sho1* gene is fused to *egfp* via a linker encoding the amino acids PVAIERANAAT. Prior to transformation and integration in the *sho1* locus, the plasmid was digested with *HindIII*.

To construct a C-terminal fusion of Msb2 to the red fluorescent protein mCherry (Shaner et al., 2004), the 0.7-kb *NcoI/BsrGI* fragment of pMF5-n (Becht et al., 2006) corresponding to *egfp* was replaced with a 0.7-kb *NcoI/BsrGI* mCherry fragment (kindly provided by M. Bölker) resulting

in pMF5-mCherry. A 1.0-kb fragment corresponding to the 3' coding region of *msb2* was amplified with the primer pair oAM331/oAM284 (5'-CACGCGCCGTTGGCCCCGGTGGCGATCGAGCGAAGGAGAACCGAGTTGCTCATC-3'/5'-GACGGCGCAATCTTTGCAT-3'), and a second 1.0-kb fragment was generated by PCR with the primers oAM332 (5'-GTTGGCCTGAGTGGCCATCTAGTTTGGTCTCTTTT-3') and oAM333 (5'-GCATTGAGTCGGCGTCCCATCCAGC-3'). Both fragments were digested with *SfiI* and ligated with the 2.4-kb *SfiI* fragment from pMF5-mCherry. After cloning this construct into pCR4-TOPO (Invitrogen), the resulting plasmid pmsb2-mCherry was digested with *SnaBI* and *PmeI* and transformed in SG200sho1GFP. In the resulting strain SG200sho1GFP/msb2mCherry, the native *msb2* gene is fused to *mcherry* via a linker encoding the amino acids RSIATGANAAT, and this is followed by the *nos* terminator and the nourseothricin resistance cassette.

For overexpression of *msb2-ha-mcherry-ha*, first pONG was constructed. Using primers oDL114 (5'-AATACCATGGTGAAGGCGCAGGAGG-3'), oDL115 (5'-TATGCGCCGCTTTAAGCGTAATCTGGAACATCGTATGGTA-3'), and pP_{otef}:vcp1-mCherryHA (A. Djamei and R. Kahmann, unpublished data) as template, a 0.7-kb product containing the *mcherry-ha* gene was amplified and digested with *NcoI* and *NotI*. pP_{otef}:vcp1-mCherryHA is a plasmid in which the secreted effector gene *vcp1* is fused to the *otef* promoter and a C-terminal *mcherry-ha* tag. A second PCR with the primer pair oD111/oD112 (5'-ATAGGATCCAGGCCTGAGTGGCCATGACAGAGGACTCTGTGCTTTATCCG-3'/5'-TTATCCATGGTGGCCGCGTTGGCCCTAGGAGCTGCATGTAGTTGCTGGG-3') using p123P_{sho1}:sho1 as template amplified a part of the *sho1* gene. The 0.6-kb product was digested with *BamHI* and *NcoI*. A three-fragment ligation with the two fragments mentioned above and the 5.5-kb *BamHI/NotI* fragment of p123 was performed to yield pONG. In pONG, the *sho1* part flanked by *SfiI* sites serves as stuffer for the integration of genes to be fused to *mcherry-ha*. To insert *msb2-ha* into pONG, the primer combinations oDL79 (5'-[P]GTGCCGACTATGCCGGCCAGTCCCTCCACTGCTCCCTCGT-3')/oDL125 (5'-TATGCGCCGCTTTGGCCGCAAGGAGAACCAGATTGCTCATC-3') and oDL80 (5'-[P]GTGCTAGGGGTAGGCTGCGCGCTGTCATCATCGCTGC-3')/oDL124 (5'-ATAGGCCTGAGTGGCCATGTTCTGTTCGACCAAC-3') using p123P_{msb2}:msb2 as template generated two PCR products, 2.2 and 1.3 kb in length, respectively. Both fragments were cut with *SfiI* and ligated with the 6.3-kb *SfiI* fragment of pONG, resulting in pP_{otef}:msb2HA-mCherryHA. In this plasmid, the *msb2* gene with an internal *ha* tag (corresponding to amino acid 421) is C-terminally fused to *mcherry-ha*. Expression of the fusion gene is driven by the *otef* promoter. pP_{otef}:msb2HA-mCherryHA was linearized with *Ssp1* and integrated into the *ip* locus of SG200Δmsb2 and SG200sho1GFP. To delete the transmembrane domain of *msb2*, a 9.7-kb fragment was amplified with the primer pair oDL197 (5'-[P]TGGCGCAAGCATCGCAAGG-3')/oDL198 (5'-[P]ACTGTTGCGCAGCGTCGAGTC-3') using pP_{otef}:msb2HA-mCherryHA as template. The resulting fragment was circularized to yield pP_{otef}:msb2HAΔTM-mCherryHA. This plasmid was linearized with *Ssp1* and integrated in single copy in the *ip* locus of SG200Δmsb2.

To express *kpp6* in *U. maydis*, pP_{otef}:kpp6NA (Brachmann, 2001) was used as progenitor plasmid. This plasmid is a derivative of pkpp6NA (Brachmann et al., 2003), constructed by exchange of almost the complete *kpp6* promoter (region -2371 to -82) with the 873-bp *otef* promoter from pOTEF-SG (Spellig et al., 1996). pP_{otef}:kpp6NA contains the *otef* promoter, followed by 81-bp 5' untranslated region, the complete ORF, and 435-bp 3' untranslated region of *kpp6*. To integrate *myc*-tagged versions of *kpp6*, three PCR reactions with the primer pair oDL131 (5'-ATACCCGGGATGGAGGAGCAGAAGCTGATCTC-3')/oDL132 (5-TATGCGCCGCTCAACGAAGAAGCGGCTGAAATTC-3') were performed, using pGBKT7-kpp6, pGBKT7-kpp6¹⁷⁰⁻⁵³³, and pGBKT7-kpp6^{P130A P131A} (see Supplemental Methods online) as templates. The

PCR products (1.1, 1.1, and 0.6 kb, respectively) were digested with *SmaI* and *BspEI* and separately ligated with the 6.0 *BspEI/SmaI* fragment of pP_{otef}:kpp6NA, resulting in pP_{otef}:myc-kpp6, pP_{otef}:myc-kpp6^{Δ1-169}, and pP_{otef}:myc-kpp6^{P130A P131A}. The plasmids were digested with *Ssp1* and integrated in single copy into the *ip* locus of SG200Δkpp6 (Brachmann et al., 2003) and SG200Δsho1 Δkpp6, respectively. The plasmid pP_{otef}:myc-kpp6 was also integrated in the *ip* locus of SG200Δkpp6 and SG200sho1-GFP in multiple copy.

The triple deletion strain of *sho1*, *msb2*, and *rok1* was constructed by linearization of pΔrok1-Cbx (Di Stasio et al., 2009) with *PvuI* and subsequent transformation into SG200Δsho1 Δmsb2.

To generate strains carrying the *fuz7DD* allele under the control of the *crg1* promoter, p123P_{crg1}:fuz7DD (Müller et al., 2003) was linearized with *AgeI* and integrated in single copy in the *ip* locus of SG200 and SG200Δsho1 Δmsb2, respectively.

For construction of *sho1* and *msb2* mutants containing the AM1 reporter gene, pAM1 (Mendoza-Mendoza et al., 2009b) was linearized with *AgeI* and transformed in SG200Δsho1, SG200Δmsb2, and SG200Δsho1 Δmsb2, respectively. Single-copy integrations of the AM1 marker in the *ip* locus were selected.

Plant Infections

Solopathogenic strains were grown in YEPSL medium to an OD₆₀₀ of 0.8 and concentrated in water to a final OD₆₀₀ of 1.0. This suspension was inoculated into 7-d-old seedlings of Early Golden Bantam (Olds Seeds). Compatible haploid strains were mixed (1:1) prior to infection. Disease symptoms were evaluated according to the disease rating criteria reported by Kämper et al. (2006). Three independent experiments were performed, and the average values (for each symptom category) were expressed as a percentage of the total number of infected plants.

Induction of Filaments and Appressoria

The in vitro system for inducing filaments and appressoria in *U. maydis* was applied as described previously (Mendoza-Mendoza et al., 2009b) with minor modifications. Briefly, SG200 and derivatives were grown in YEPSL at 28°C to an OD₆₀₀ of 0.6 to 0.8. The cells were resuspended in 2% YEPSL to an OD₆₀₀ of 0.2 and supplemented with either 100 μM (f.c.) 16-hydroxyhexadecanoic acid (Sigma-Aldrich) or an appropriate amount of ethanol (1%, f.c.), the solvent of 16-hydroxyhexadecanoic acid. For filament induction in liquid, the samples were incubated at 28°C on a rotating wheel, and after 18 h the number of cells that had developed filaments relative to the number of total cells was determined using light microscopy. To quantify filament formation on a hydrophobic surface, cells were sprayed (EcoSpray Labo Chimie) on Parafilm M and incubated at 100% humidity at 28°C for 18 h. The samples were stained with calcofluor to visualize fungal cells, and the percentage of cells that had developed filaments relative to total cells was determined using fluorescence microscopy. For appressoria quantification, SG200AM1 derivatives were inoculated into 7-d-old maize seedlings 2 cm above ground or were sprayed on Parafilm M, as described above. After 18 h, the third leaf of infected plants was prepared, washed with water, and stained with calcofluor (Sigma-Aldrich). Likewise, the Parafilm M samples were washed with water and stained. Using fluorescence microscopy, filaments expressing the AM1 marker that is expressed in cells forming appressoria were visualized by their GFP fluorescence, and the ratio of appressoria to filamentous cells was determined. All experiments were performed in three biological replicates.

To visualize Sho1-GFP and Msb2-mCherryHA in appressoria, a flat hydrophobic surface lacking background fluorescence was generated by melting and casting Granopent P (Carl Roth).

Microscopy

For analysis of *U. maydis* sporidia, cells were grown at 28°C to an OD₆₀₀ of 0.6. Latrunculin A (Sigma-Aldrich) was applied at a final concentration of 10 μM following a 2-h incubation at room temperature. To stain fungal material, samples were incubated in calcofluor Fluorescent Brightner 28 (100 μg/mL in 0.2 M Tris/HCl, pH 8.0; Sigma-Aldrich) for 30 s. For staining of plant cells with propidium iodide (Sigma-Aldrich), fresh leaves were incubated in 10 μg/mL propidium iodide (in PBS, pH 7.4) for 20 min. To examine fungal colonization inside the leaf tissue 6 d after infection, the third oldest leaf was destained in ethanol, transferred to 10% KOH, incubated at 95°C overnight, washed once with PBS buffer (140 mM NaCl, 16 mM Na₂HPO₄, 2 mM KH₂PO₄, 3.5 mM KCl, and 1 mM Na₂-EDTA, pH 7.4), and incubated under vacuum in staining solution (10 μg/mL propidium iodide and 10 μg/mL WGA-AF 488 in PBS, pH 7.4) according to Doehlemann et al. (2008b). WGA-AF 488 was purchased from Invitrogen.

For microscopy, an Axioplan II microscope (Zeiss) with differential interference contrast optics was used. Fluorescence of GFP, mCherry, and calcofluor was observed using GFP (ET470/40BP, ET495LP, and ET525/50BP), TexasRed (HC562/40BP, HC593LP, and HC624/40BP), and 4',6-diamidino-2-phenylindole (HC375/11BP, HC409BS, and HC447/60BP) filter sets (Semrock). Pictures were taken with a CoolSNAP-HQ charge-coupled device camera (Photometrics). Image processing was done with MetaMorph software (Universal Imaging).

Confocal microscopy was performed using a TCS-SP5 confocal microscope (Leica Microsystems). For GFP fluorescence, an excitation of 488 nm and detection at 495–530 nm was used. Propidium iodide and mCherry fluorescence was excited with 561 nm and detected at 580–630 nm. To visualize WGA-AF 488, an excitation of 488 nm and subsequent detection at 500–540 nm was employed. Calcofluor and autofluorescence were excited with a 405 nm laser and detected at 415–460 nm. Images were processed using LAS-AF software (Leica Microsystems).

Quantitative Real-Time PCR

An iCycler-machine (Bio-Rad) in combination with Platinum SYBR Green qPCR SuperMix-UDG (Invitrogen) was used. For data analysis, iCycler software (Bio-Rad) was used.

To determine fungal biomass after infection, we followed the procedure described by Di Stasio et al. (2009), with some modifications. Briefly, plants were inoculated with the solopathogenic strains SG200, SG200Δ*sho1*, SG200Δ*msb2*, and SG200Δ*sho1* Δ*msb2*, and 3 d after inoculation, the third oldest leaf was prepared. Fungal cells on the leaf surface were peeled off by applying liquid latex (Orion). Subsequently, 4-cm-long sections below the injection holes were excised, and 10 excised sections were pooled. From this material, total DNA was extracted as described by Di Stasio et al. (2009). Quantitative real-time PCR analysis was conducted with primer pairs *mfa1*-RT-FW (5'-GCTTTCGATC-TTCGCTCAGAC-3')/*mfa1*-RT-RV (5'-CAACAACACAGCTGGAGTAGC-3') for detecting *U. maydis* DNA and *Gapdh*-FW (5'-CTTCGGCATTGTT-GAGGGTTTG-3')/*Gapdh*-RV (5'-TCCTTGCTGAGGGTCCGTC-3') for detection of maize DNA. The experiment was done in three biological replicates, and the ratio of SG200 DNA to plant DNA was set to 1.0.

Molecular Techniques

For molecular analysis, standard procedures were followed (Sambrook et al., 1989). Transformation of *U. maydis* was performed as published previously (Schulz et al., 1990), and DNA was isolated according to the protocol of Hoffman and Winston (1987). For extraction of proteins from *S. cerevisiae*, 10 mL of cells (OD₆₀₀ of 1.0) were washed with 50 mM Tris/HCl, pH 7.5, and resuspended in 100 μL ESB buffer (80 mM Tris-HCl, pH 8.0, 2% SDS, 10% glycerol, 100 mM DTT, and 0.01% bromophenol blue).

Samples were boiled for 3 min at 95°C and supplemented with glass beads, and cells were disrupted by incubation for 3 min on a Vibrax shaker (IKA). After additional boiling (1 min at 95°C), samples were subjected to SDS polyacrylamide electrophoresis. For isolation of proteins from *U. maydis*, 2 mL of cells (OD₆₀₀ of 1.0) were washed in water and resuspended in 100 μL Thorer buffer (8 M urea, 5% SDS, 0.1 mM EDTA, 0.01% bromophenol blue, 100 mM DTT, and 100 mM Tris-HCl, pH 6.8). Samples were boiled for 10 min at 95°C, supplemented with glass beads, and incubated 5 min on a Vibrax shaker (IKA). After a second boiling step (10 min at 95°C), 10 μL was loaded for SDS polyacrylamide gel electrophoresis. Transfer of proteins to PVDF nitrocellulose membranes (Amersham Pharmacia Biotech) was conducted in a semidry blot chamber (UniEquip). Blots were probed with monoclonal GAL4-DBD, GAL4-TA (both Santa Cruz Biotechnology), anti-HA (Sigma-Aldrich), anti-c-Myc (Sigma-Aldrich), anti-GFP (Roche), and antitubulin (Merck) antibodies. To detect mCherry, a rabbit serum against RFP was used (kindly provided by M. Thanbichler). Horseradish peroxidase-conjugated anti-mouse or anti-rabbit IgG (Cell Signaling) was used as secondary antibody, and the ECL Plus System (Amersham Pharmacia Biotech) was used for protein detection.

Accession Numbers

Sequence data from this article can be found at GenBank/EMBL databases under accession numbers XP_759303 (*sho1*) and XP_756627 (*msb2*).

Supplemental Data

The following materials are available in the online version of this article.

- Supplemental Figure 1.** Schematic Illustration of Signaling Cascades in *U. maydis* and *S. cerevisiae*.
- Supplemental Figure 2.** Sho1-GFP and Msb2-mCherry Fusions Are Functional.
- Supplemental Figure 3.** Sho1 and Msb2 Are Membrane Associated.
- Supplemental Figure 4.** Sho1 Interacts Specifically with Kpp6.
- Supplemental Figure 5.** Pathogenicity of Haploid *sho1* and *msb2* Mutant Strains after Mating.
- Supplemental Figure 6.** Stress Response in *sho1* and *msb2* Mutants.
- Supplemental Figure 7.** SG200Δ*sho1* Δ*msb2* Induces Plant Cell Death.
- Supplemental Figure 8.** Hydroxy Fatty Acids Induce Filamentation in *sho1* and *msb2* Mutants.
- Supplemental Figure 9.** Hydrophobic Surface-Induced Differentiation in *sho1* and *msb2* Mutants.
- Supplemental Figure 10.** The Transmembrane Domain of Msb2 Is Essential for Function.
- Supplemental Figure 11.** *U. maydis* Msb2 Cannot Functionally Replace *S. cerevisiae* Msb2p.
- Supplemental Figure 12.** The SH3 Domain of Sho1 Interacts with the N Terminus of Kpp6.
- Supplemental Figure 13.** The SH3 Domain of Sho1 Is Essential for Function.
- Supplemental Table 1.** *S. cerevisiae* Strains Used in This Study.
- Supplemental Table 2.** *U. maydis* Strains Used in This Study.
- Supplemental Methods.** Two-Hybrid Interaction Studies, Complementation of the *S. cerevisiae* *msb2* Mutant, Stress Assays,

Coimmunoprecipitation Analysis, and Subcellular Fractionation of Proteins.

Supplemental References.

ACKNOWLEDGMENTS

We thank X. Xia for help with plasmid and strain constructions, A. Djamei and G. Doehlemann for help with confocal microscopy, and P. Berndt and J. Freitag for stimulating discussions. We thank E. Perez-Nadales and A. Di Pietro for communicating results prior to publication, P. J. Cullen for providing yeast strains, M. Bölker for providing the *mcherry* gene, and M. Thanbichler for antibodies. D.L. was supported through the International Max Planck Research School and the GRK1216. We acknowledge support through the EU network Signal-path.

Received January 5, 2010; revised May 3, 2010; accepted June 11, 2010; published June 29, 2010.

REFERENCES

- Aichinger, C., Hansson, K., Eichhorn, H., Lessing, F., Mannhaupt, G., Mewes, W., and Kahmann, R. (2003). Identification of plant-regulated genes in *Ustilago maydis* by enhancer-trapping mutagenesis. *Mol. Genet. Genomics* **270**: 303–314.
- Andrews, D.L., Egan, J.D., Mayorga, M.E., and Gold, S.E. (2000). The *Ustilago maydis* *ubc4* and *ubc5* genes encode members of a MAP kinase cascade required for filamentous growth. *Mol. Plant Microbe Interact.* **13**: 781–786.
- Banuett, F., and Herskowitz, I. (1989). Different alleles of *Ustilago maydis* are necessary for maintenance of filamentous growth but not for meiosis. *Proc. Natl. Acad. Sci. USA* **86**: 5878–5882.
- Banuett, F., and Herskowitz, I. (1994). Identification of *fuz7*, a *Ustilago maydis* MEK/MAPKK homolog required for *a*-locus-dependent and -independent steps in the fungal life cycle. *Genes Dev.* **8**: 1367–1378.
- Bechinger, C., Giebel, K.F., Schnell, M., Leiderer, P., Deising, H.B., and Bastmeyer, M. (1999). Optical measurements of invasive forces exerted by appressoria of a plant pathogenic fungus. *Science* **285**: 1896–1899.
- Becht, P., König, J., and Feldbrugge, M. (2006). The RNA-binding protein Rrm4 is essential for polarity in *Ustilago maydis* and shuttles along microtubules. *J. Cell Sci.* **119**: 4964–4973.
- Boisnard, S., Ruprich-Robert, G., Florent, M., Da Silva, B., Chapeland-Leclerc, F., and Papon, N. (2008). Role of Sho1p adaptor in the pseudohyphal development, drug sensitivity, osmotolerance and oxidant stress adaptation in the opportunistic yeast *Candida lusitanae*. *Yeast* **25**: 849–859.
- Bölker, M., Urban, M., and Kahmann, R. (1992). The *a* mating type locus of *U. maydis* specifies cell signaling components. *Cell* **68**: 441–450.
- Bottin, A., Kämper, J., and Kahmann, R. (1996). Isolation of a carbon source-regulated gene from *Ustilago maydis*. *Mol. Gen. Genet.* **13**: 342–352.
- Brachmann, A. (2001). Die frühe Infektionsphase von *Ustilago maydis*: Genregulation durch das bW/bE-Heterodimer. PhD dissertation (Munich, Germany: Ludwig-Maximilians-University).
- Brachmann, A., König, J., Julius, C., and Feldbrugge, M. (2004). A reverse genetic approach for generating gene replacement mutants in *Ustilago maydis*. *Mol. Genet. Genomics* **272**: 216–226.
- Brachmann, A., Schirawski, J., Müller, P., and Kahmann, R. (2003). An unusual MAP kinase is required for efficient penetration of the plant surface by *Ustilago maydis*. *EMBO J.* **22**: 2199–2210.
- Brewster, J.L., de Valoir, T., Dwyer, N.D., Winter, E., and Gustin, M.C. (1993). An osmosensing signal transduction pathway in yeast. *Science* **259**: 1760–1763.
- Chen, R.E., and Thorner, J. (2007). Function and regulation in MAPK signaling pathways: Lessons learned from the yeast *Saccharomyces cerevisiae*. *Biochim. Biophys. Acta* **1773**: 1311–1340.
- Choi, W., and Dean, R.A. (1997). The adenylate cyclase gene *MAC1* of *Magnaporthe grisea* controls appressorium formation and other aspects of growth and development. *Plant Cell* **9**: 1973–1983.
- Cullen, P.J. (2007). Signaling mucins: The new kids on the MAPK block. *Crit. Rev. Eukaryot. Gene Expr.* **17**: 241–257.
- Cullen, P.J., Sabbagh, W., Jr., Graham, E., Irick, M.M., van Olden, E.K., Neal, C., Delrow, J., Bardwell, L., and Sprague, G.F., Jr. (2004). A signaling mucin at the head of the Cdc42- and MAPK-dependent filamentous growth pathway in yeast. *Genes Dev.* **18**: 1695–1708.
- DeZwaan, T.M., Carroll, A.M., Valent, B., and Sweigard, J.A. (1999). *Magnaporthe grisea* pth11p is a novel plasma membrane protein that mediates appressorium differentiation in response to inductive substrate cues. *Plant Cell* **11**: 2013–2030.
- De Nadal, E., Real, F.X., and Posas, F. (2007). Mucins, osmosensors in eukaryotic cells? *Trends Cell Biol.* **17**: 571–574.
- Di Stasio, M., Brefort, T., Mendoza-Mendoza, A., Munch, K., and Kahmann, R. (2009). The dual specificity phosphatase Rok1 negatively regulates mating and pathogenicity in *Ustilago maydis*. *Mol. Microbiol.* **73**: 73–88.
- Doehlemann, G., Berndt, P., and Hahn, M. (2006). Different signalling pathways involving a Galpha protein, cAMP and a MAP kinase control germination of *Botrytis cinerea* conidia. *Mol. Microbiol.* **59**: 821–835.
- Doehlemann, G., van der Linde, K., Assmann, D., Schwambach, D., Hof, A., Mohanty, A., Jackson, D., and Kahmann, R. (2009). Pep1, a secreted effector protein of *Ustilago maydis*, is required for successful invasion of plant cells. *PLoS Pathog.* **5**: e1000290.
- Doehlemann, G., Wahl, R., Horst, R.J., Voll, L.M., Usadel, B., Poree, F., Stitt, M., Pons-Kuhnemann, J., Sonnwald, U., Kahmann, R., and Kamper, J. (2008a). Reprogramming a maize plant: Transcriptional and metabolic changes induced by the fungal biotroph *Ustilago maydis*. *Plant J.* **56**: 181–195.
- Doehlemann, G., Wahl, R., Vranes, M., de Vries, R.P., Kamper, J., and Kahmann, R. (2008b). Establishment of compatibility in the *Ustilago maydis*/maize pathosystem. *J. Plant Physiol.* **165**: 29–40.
- Feldbrugge, M., Kamper, J., Steinberg, G., and Kahmann, R. (2004). Regulation of mating and pathogenic development in *Ustilago maydis*. *Curr. Opin. Microbiol.* **7**: 666–672.
- Fernandez-Alvarez, A., Elias-Villalobos, A., and Ibeas, J.I. (2009). The O-mannosyltransferase PMT4 is essential for normal appressorium formation and penetration in *Ustilago maydis*. *Plant Cell* **21**: 3397–3412.
- Fuchs, U., Hause, G., Schuchardt, I., and Steinberg, G. (2006). Endocytosis is essential for pathogenic development in the corn smut fungus *Ustilago maydis*. *Plant Cell* **18**: 2066–2081.
- Gimeno, C.J., Ljungdahl, P.O., Styles, C.A., and Fink, G.R. (1992). Unipolar cell division in the yeast *S. cerevisiae* lead to filamentous growth: Regulation by starvation and RAS. *Cell* **68**: 1077–1090.
- Hao, N., Behar, M., Parnell, S.C., Torres, M.P., Borchers, C.H., Elston, T.C., and Dohlman, H.G. (2007). A systems-biology analysis of feedback inhibition in the Sho1 osmotic-stress-response pathway. *Curr. Biol.* **17**: 659–667.
- Hoffman, C.S., and Winston, F. (1987). A ten-minute DNA preparation

- from yeast efficiently releases autonomous plasmids for transformation of *E. coli*. *Gene* **57**: 267–272.
- Holliday, R.** (1974). *Ustilago maydis*. In Handbook of Genetics, R.C. King, ed (New York: Plenum Press), pp. 575–595.
- Hollingsworth, M.A., and Swanson, B.J.** (2004). Mucins in cancer: Protection and control of the cell surface. *Nat. Rev. Cancer* **4**: 45–60.
- Howard, R.J., Ferrari, M.A., Roach, D.H., and Money, N.P.** (1991). Penetration of hard substrates by a fungus employing enormous turgor pressures. *Proc. Natl. Acad. Sci. USA* **88**: 11281–11284.
- Kämper, J.** (2004). A PCR-based system for highly efficient generation of gene replacement mutants in *Ustilago maydis*. *Mol. Genet. Genomics* **271**: 103–110.
- Kämper, J., et al.** (2006). Insights from the genome of the biotrophic fungal plant pathogen *Ustilago maydis*. *Nature* **444**: 97–101.
- Kim, Y.K., Liu, Z.M., Li, D., and Kolattukudy, P.E.** (2000). Two novel genes induced by hard-surface contact of *Colletotrichum gloeosporioides* conidia. *J. Bacteriol.* **182**: 4688–4695.
- Krantz, M., Becit, E., and Hohmann, S.** (2006). Comparative genomics of the HOG-signalling system in fungi. *Curr. Genet.* **49**: 137–151.
- Kumamoto, C.A.** (2008). Molecular mechanisms of mechanosensing and their roles in fungal contact sensing. *Nat. Rev. Microbiol.* **6**: 667–673.
- Lee, Y.H., and Dean, R.A.** (1993). cAMP regulates infection structure formation in the plant pathogenic fungus *Magnaporthe grisea*. *Plant Cell* **5**: 693–700.
- Lev, S., Sharon, A., Hadar, R., Ma, H., and Horwitz, B.A.** (1999). A mitogen-activated protein kinase of the corn leaf pathogen *Cochliobolus heterostrophus* is involved in conidiation, appressorium formation, and pathogenicity: Diverse roles for mitogen-activated protein kinase homologs in foliar pathogens. *Proc. Natl. Acad. Sci. USA* **96**: 13542–13547.
- Leveleki, L., Mählert, M., Sandrock, B., and Bolker, M.** (2004). The PAK family kinase Cla4 is required for budding and morphogenesis in *Ustilago maydis*. *Mol. Microbiol.* **54**: 396–406.
- Li, S.S.** (2005). Specificity and versatility of SH3 and other proline-recognition domains: Structural basis and implications for cellular signal transduction. *Biochem. J.* **390**: 641–653.
- Liu, H., Styles, C.A., and Fink, G.R.** (1993). Elements of the yeast pheromone response pathway required for filamentous growth of diploids. *Science* **262**: 1741–1744.
- Loubradou, G., Brachmann, A., Feldbrugge, M., and Kahmann, R.** (2001). A homologue of the transcriptional repressor Ssn6p antagonizes cAMP signalling in *Ustilago maydis*. *Mol. Microbiol.* **40**: 719–730.
- Ma, Y., Qiao, J., Liu, W., Wan, Z., Wang, X., Calderone, R., and Li, R.** (2008). The sho1 sensor regulates growth, morphology, and oxidant adaptation in *Aspergillus fumigatus* but is not essential for development of invasive pulmonary aspergillosis. *Infect. Immun.* **76**: 1695–1701.
- Maeda, T., Takekawa, M., and Saito, H.** (1995). Activation of yeast PBS2 MAPKK by MAPKKs or by binding of an SH3-containing osmosensor. *Science* **269**: 554–558.
- Mählert, M., Leveleki, L., Hlubek, A., Sandrock, B., and Bolker, M.** (2006). Rac1 and Cdc42 regulate hyphal growth and cytokinesis in the dimorphic fungus *Ustilago maydis*. *Mol. Microbiol.* **59**: 567–578.
- Mayorga, M.E., and Gold, S.E.** (1999). A MAP kinase encoded by the *ubc3* gene of *Ustilago maydis* is required for filamentous growth and full virulence. *Mol. Microbiol.* **34**: 485–497.
- Mendoza-Mendoza, A., Berndt, P., Djamei, A., Weise, C., Linne, U., Marahiel, M., Vranes, M., Kamper, J., and Kahmann, R.** (2009b). Physical-chemical plant-derived signals induce differentiation in *Ustilago maydis*. *Mol. Microbiol.* **71**: 895–911.
- Mendoza-Mendoza, A., Eskova, A., Weise, C., Czajkowski, R., and Kahmann, R.** (2009a). Hap2 regulates the pheromone response transcription factor *prf1* in *Ustilago maydis*. *Mol. Microbiol.* **72**: 683–698.
- Müller, P., Aichinger, C., Feldbrugge, M., and Kahmann, R.** (1999). The MAP kinase *kpp2* regulates mating and pathogenic development in *Ustilago maydis*. *Mol. Microbiol.* **34**: 1007–1017.
- Müller, P., Weinzierl, G., Brachmann, A., Feldbrugge, M., and Kahmann, R.** (2003). Mating and pathogenic development of the smut fungus *Ustilago maydis* are regulated by one mitogen-activated protein kinase cascade. *Eukaryot. Cell* **2**: 1187–1199.
- Norice, C.T., Smith, F.J., Jr., Solis, N., Filler, S.G., and Mitchell, A.P.** (2007). Requirement for *Candida albicans* Sun41 in biofilm formation and virulence. *Eukaryot. Cell* **6**: 2046–2055.
- O'Rourke, S.M., and Herskowitz, I.** (1998). The Hog1 MAPK prevents cross talk between the HOG and pheromone response MAPK pathways in *Saccharomyces cerevisiae*. *Genes Dev.* **12**: 2874–2886.
- O'Rourke, S.M., and Herskowitz, I.** (2002). A third osmosensing branch in *Saccharomyces cerevisiae* requires the Msb2 protein and functions in parallel with the Sho1 branch. *Mol. Cell. Biol.* **22**: 4739–4749.
- Pitoniak, A., Birkaya, B., Dionne, H.M., Vadaie, N., and Cullen, P. J.** (2009). The signaling mucins Msb2 and Hkr1 differentially regulate the filamentation mitogen-activated protein kinase pathway and contribute to a multimodal response. *Mol. Biol. Cell* **13**: 3101–3114.
- Posas, F., and Saito, H.** (1997). Osmotic activation of the HOG MAPK pathway via Ste11p MAPKKK: Scaffold role of Pbs2p MAPKK. *Science* **276**: 1702–1705.
- Raitt, D.C., Posas, F., and Saito, H.** (2000). Yeast Cdc42 GTPase and Ste20 PAK-like kinase regulate Sho1-dependent activation of the Hog1 MAPK pathway. *EMBO J.* **19**: 4623–4631.
- Reiser, V., Salah, S.M., and Ammerer, G.** (2000). Polarized localization of yeast Pbs2 depends on osmotic stress, the membrane protein Sho1 and Cdc42. *Nat. Cell Biol.* **2**: 620–627.
- Roberts, R.L., and Fink, G.R.** (1994). Elements of a single MAP kinase cascade in *Saccharomyces cerevisiae* mediate two developmental programs in the same cell type: Mating and invasive growth. *Genes Dev.* **8**: 2974–2985.
- Roman, E., Cottier, F., Ernst, J.F., and Pla, J.** (2009). Msb2 signaling mucin controls activation of Cek1 mitogen-activated protein kinase in *Candida albicans*. *Eukaryot. Cell* **8**: 1235–1249.
- Roman, E., Nombela, C., and Pla, J.** (2005). The Sho1 adaptor protein links oxidative stress to morphogenesis and cell wall biosynthesis in the fungal pathogen *Candida albicans*. *Mol. Cell. Biol.* **25**: 10611–10627.
- Ruiz-Roldan, M.C., Maier, F.J., and Schafer, W.** (2001). PTK1, a mitogen-activated-protein kinase gene, is required for conidiation, appressorium formation, and pathogenicity of *Pyrenophora teres* on barley. *Mol. Plant Microbe Interact.* **14**: 116–125.
- Sambrook, J., Fritsch, E.F., and Maniatis, T.** (1989). *Molecular Cloning: A Laboratory Manual*. (Cold Spring Harbor, NY: Cold Spring Harbor Laboratory Press).
- Schirawski, J., Bohnert, H.U., Steinberg, G., Snetselaar, K., Adamikowa, L., and Kahmann, R.** (2005). Endoplasmic reticulum glucosidase II is required for pathogenicity of *Ustilago maydis*. *Plant Cell* **17**: 3532–3543.
- Schulz, B., Banuett, F., Dahl, M., Schlesinger, R., Schäfer, W., Martin, T., Herskowitz, I., and Kahmann, R.** (1990). The *b* alleles of *U. maydis*, whose combinations program pathogenic development, code for polypeptides containing a homeodomain-related motif. *Cell* **60**: 295–306.
- Seet, B.T., and Pawson, T.** (2004). MAPK signaling: Sho business. *Curr. Biol.* **14**: R708–R710.
- Shaner, N.C., Campbell, R.E., Steinbach, P.A., Giepmans, B.N.,**

- Palmer, A.E., and Tsien, R.Y.** (2004). Improved monomeric red, orange and yellow fluorescent proteins derived from *Discosoma* sp. red fluorescent protein. *Nat. Biotechnol.* **22**: 1567–1572.
- Singh, P.K., and Hollingsworth, M.A.** (2006). Cell surface-associated mucins in signal transduction. *Trends Cell Biol.* **16**: 467–476.
- Smith, D.G., Garcia-Pedrajas, M.D., Gold, S.E., and Perlin, M.H.** (2003). Isolation and characterization from pathogenic fungi of genes encoding ammonium permeases and their roles in dimorphism. *Mol. Microbiol.* **50**: 259–275.
- Snetselaar, K.M., and Mims, C.W.** (1992). Sporidial fusion and infection of maize seedlings by the smut fungus *Ustilago maydis*. *Mycologia* **84**: 193–203.
- Spellig, T., Bottin, A., and Kahmann, R.** (1996). Green fluorescent protein (GFP) as a new vital marker in the phytopathogenic fungus *Ustilago maydis*. *Mol. Gen. Genet.* **252**: 503–509.
- Takano, Y., Kikuchi, T., Kubo, Y., Hamer, J.E., Mise, K., and Furusawa, I.** (2000). The *Colletotrichum lagenarium* MAP kinase gene CMK1 regulates diverse aspects of fungal pathogenesis. *Mol. Plant Microbe Interact.* **13**: 374–383.
- Tatebayashi, K., Tanaka, K., Yang, H.Y., Yamamoto, K., Matsushita, Y., Tomida, T., Imai, M., and Saito, H.** (2007). Transmembrane mucins Hkr1 and Msb2 are putative osmosensors in the SHO1 branch of yeast HOG pathway. *EMBO J.* **26**: 3521–3533.
- Tucker, S.L., and Talbot, N.J.** (2001). Surface attachment and pre-penetration stage development by plant pathogenic fungi. *Annu. Rev. Phytopathol.* **39**: 385–417.
- Vadaie, N., Dionne, H., Akajagbor, D.S., Nickerson, S.R., Krysan, D.J., and Cullen, P.J.** (2008). Cleavage of the signaling mucin Msb2 by the aspartyl protease Yps1 is required for MAPK activation in yeast. *J. Cell Biol.* **181**: 1073–1081.
- Weinzierl, G., Leveleki, L., Hassel, A., Kost, G., Wanner, G., and Bolker, M.** (2002). Regulation of cell separation in the dimorphic fungus *Ustilago maydis*. *Mol. Microbiol.* **45**: 219–231.
- Xu, J.R., and Hamer, J.E.** (1996). MAP kinase and cAMP signaling regulate infection structure formation and pathogenic growth in the rice blast fungus *Magnaporthe grisea*. *Genes Dev.* **10**: 2696–2706.
- Yang, H.Y., Tatebayashi, K., Yamamoto, K., and Saito, H.** (2009). Glycosylation defects activate filamentous growth Kss1 MAPK and inhibit osmoregulatory Hog1 MAPK. *EMBO J.* **28**: 1380–1391.
- Zhao, X., Kim, Y., Park, G., and Xu, J.R.** (2005). A mitogen-activated protein kinase cascade regulating infection-related morphogenesis in *Magnaporthe grisea*. *Plant Cell* **17**: 1317–1329.